

ν_μ disappearance at the SPL, T2K-I, NO ν A and the Neutrino Factory

A. Donini^a E. Fernández-Martínez^a D. Meloni^b S. Rigolin^a

^a*I.F.T. and Dep. Física Teórica, Univ. Autónoma Madrid., E-28049, Madrid, Spain*

^b*INFN, Sezione di Roma e Dip. di Fisica, Univ. di Roma “La Sapienza”, P.le A. Moro 2, I-00185 Roma, Italy*

PACS: 14.60.Pq, 14.60.Lm

Abstract

We study the measurement of the atmospheric neutrino oscillation parameters, θ_{23} and Δm_{23}^2 , at the ν_μ disappearance channel at three conventional beam facilities, the SPL, T2K-phase I and NO ν A. These two parameters have been shown to be of crucial importance in the measurement of two of the unknowns of the PMNS mixing matrix, θ_{13} and the leptonic CP-violating phase δ . In our analysis, the effect of the two discrete ambiguities, $\text{sign}(\Delta m_{23}^2)$ and $\text{sign}(\tan 2\theta_{23})$, is explicitly taken into account. We analyse also the ν_μ disappearance channel at the Neutrino Factory, and combine it with the “golden” $\nu_e \rightarrow \nu_\mu$ and “silver” $\nu_e \rightarrow \nu_\tau$ appearance channels to study its impact on the measurement of θ_{13} and δ . Eventually, we present the sensitivity of the four facilities to different observables: θ_{13} , δ , maximal θ_{23} , the sign of the atmospheric mass difference, s_{atm} , and the θ_{23} -octant, s_{oct} .

1 Introduction

The results of atmospheric, solar, accelerator and reactor neutrino experiments [1] show that flavour mixing occurs not only in the hadronic sector, as it has been known for long, but in the leptonic sector as well. The experimental results point to two very distinct mass differences¹, $\Delta m_{sol}^2 \approx 8.2 \times 10^{-5} \text{ eV}^2$ and $|\Delta m_{atm}^2| \approx 2.5 \times 10^{-3} \text{ eV}^2$. Only two out of the four parameters of the three-family leptonic mixing matrix U_{PMNS} [4] are known: $\theta_{12} \approx 34^\circ$ and $\theta_{23} \approx 45^\circ$. The other two parameters, θ_{13} and δ , are still unknown: for the mixing angle θ_{13} direct searches at reactors [5] and three-family global analysis of the experimental data [6] give the upper bound $\theta_{13} \leq 11.5^\circ$, whereas for the leptonic CP-violating phase δ we have no information whatsoever. Two additional discrete unknowns are the sign of the atmospheric mass difference and the θ_{23} -octant (if $\theta_{23} \neq 45^\circ$).

The full understanding of the leptonic mixing matrix constitutes, together with the discrimination of the Dirac/Majorana character of neutrinos and with the measurement of their absolute mass scale, the main neutrino-physics goal for the next decade. In the recent past, most of the experimental breakthroughs in neutrino physics have been achieved by exploiting the so-called “disappearance channels”: by observing a deficit in the neutrinos that reach the detector with respect to those expected to be emitted from the source, a positive and eventually unambiguous signal of neutrino oscillations has been established. The SK detector has gathered indirect evidence of $\nu_\mu \rightarrow \nu_\tau$ conversion of atmospheric neutrinos. However, no direct observation of τ 's is possible at this detector. To observe directly $\mu \rightarrow \tau$ conversion, two detectors are under construction at the Gran Sasso Laboratory [7,8]. The SNO experiment [9] has shown that a fraction of the ν_e 's emitted by the Sun core reach the Earth converted into ν_μ 's and ν_τ 's (and not into unobservable sterile neutrinos). However, the SNO detector is not able to distinguish between τ 's and μ 's and thus measure the subleading oscillations $\nu_e \rightarrow \nu_\tau, \nu_\mu$ directly. For this reason, new-generation experiments have been proposed to look for the fleeting and intimately related parameters θ_{13} and δ through the more promising “appearance channels” such as $\nu_e \rightarrow \nu_\mu$ or $\nu_\mu \rightarrow \nu_e$ (the “golden channel”) and $\nu_e \rightarrow \nu_\tau$ (the “silver channel”). However, strong correlations between θ_{13} and δ [10] and the presence of parametric degeneracies in the (θ_{13}, δ) parameter space, [11]-[14], make the simultaneous measurement of the two variables extremely difficult. A further problem arises from our present imprecise knowledge of atmospheric parameters, whose uncertainties are far too large to be neglected when looking for such tiny signals as those expected in appearance experiments [15]. Most of proposed solutions to these problems suggests the combination of different experiments and facilities, such as Super-Beam's (of which T2K [16] is the first approved one), β -Beam's [17] or the Neutrino Factory [18,19].

¹ A third mass difference, $\Delta m_{LSND}^2 \sim 1 \text{ eV}^2$, suggested by the LSND experiment [2], has not being confirmed yet [3] and will not be considered in this paper.

Clearly, the ν_μ disappearance channel is the best place to reduce further the uncertainties on atmospheric parameters. It must be reminded, however, that this channel is afflicted by a four-fold degeneracy [20]: the sign of the atmospheric mass difference and the θ_{23} -octant are poorly measured through this channel, indeed². It has been proposed to face this problem using atmospheric neutrinos at T2K-II, [21], or at a magnetized iron calorimeter, [22].

The study of the disappearance $\nu_\mu \rightarrow \nu_\mu$ channel at several proposed facilities is the main goal of this paper (partially presented in Ref. [23]). How the combination of appearance and disappearance channels at different facilities can be used to soften the degeneracy problem in the measurement of θ_{13} and δ is also analysed. We first study in detail the disappearance channel at three proposed SuperBeam facilities, T2K-I [16] (that is under construction at the Jaeri site), NO ν A [24] (that passed first scrutiny and will rely upon the existing NuMI facility at FermiLab) and the SPL [25]. We will show how energy resolution is crucial to reduce significantly atmospheric parameter uncertainties and how our present ignorance of θ_{13} and δ affects the results in the disappearance channel.

We then investigate the $\nu_\mu \rightarrow \nu_\mu$ disappearance channel at the Neutrino Factory. This channel, although already considered in the literature (see Refs. [26,27], for example), has never gained the center of the stage on its own, being overshadowed by appearance channels such as the “golden” $\nu_e \rightarrow \nu_\mu$ and the “silver” [28] $\nu_e \rightarrow \nu_\tau$ transitions. This channel is able to reduce atmospheric parameter uncertainties to an unprecedented level and, using the intertwine with appearance channels, to solve many of the discrete ambiguities for $\theta_{13} \geq 3^\circ - 4^\circ$. In this range of θ_{13} , combination of appearance and disappearance channels is rather effective and θ_{13} and δ can also be measured unambiguously. Unfortunately, appearance and disappearance signals are optimized with different baselines: degeneracies are solved most effectively with a $L = 3000$ km baseline in the appearance channel and with a $L = 7000$ km baseline in the disappearance channel³.

Eventually, we present a comparison of the sensitivity to θ_{13} , to the sign of the atmospheric mass difference, to the θ_{23} -octant and to maximal θ_{23} of the different facilities. Their CP-discovery potential [20] is also shown. As expected, the Neutrino Factory outperforms the considered SuperBeams in every aspect, with the notable exception of the CP-discovery potential that seems to be larger for T2K-II. The Neutrino Factory is in this case limited by the “accidental” flow of degeneracies towards $|\delta| = 0^\circ$ or 180° for very small values of θ_{13} , see Refs. [31,32].

The paper is organized as follows: in Sect. 2 we shortly introduce the four facilities and the neutrino-nucleon cross-section; in Sect. 3 we compare the potential of the three conventional beams in the measurement of the atmospheric parameters θ_{23} and Δm_{23}^2 ;

² This is why we have to deal with these ambiguities when looking to appearance signals, ultimately.

³ This was known for long (see Refs. [29] and [30] at this regard).

in Sect. 4 we study the potential of the Neutrino Factory in the measurement of the atmospheric parameters and combine the ν_μ disappearance channel with “golden” and “silver” appearance channels; in Sect. 5 we show the sensitivity to several unknowns of the considered facilities combining appearance and disappearance channels; in Sect. 6 we eventually draw our conclusions.

2 The experimental setup

In this section we describe, briefly, the four facilities that we will use in the following and we remind the neutrino-nucleon cross-section used throughout the paper.

2.1 The T2K Beam

A Super-Beam is a conventional neutrino beam with a proton intensity higher than that of existing (or under construction) beams such as K2K [33], NuMI [34] and the CNGS [35]. With respect to the β -Beam [17] and the Neutrino Factory [18], neutrino beams of a new design, it has the advantage of a well known technology. On the other hand, the flux composition (with ν_μ as the main component for a π^+ focusing, plus a small but unavoidable admixture of $\bar{\nu}_\mu$, ν_e and $\bar{\nu}_e$) limits its sensitivity to $\nu_\mu \rightarrow \nu_e$ oscillations.

The T2K-I facility [16] has been approved and it is under construction. It consists of a conventional beam with 0.75 MWatt power 50 GeV protons produced at the J-Parc site in Tokai aiming at the Super-Kamiokande water Čerenkov detector with a baseline $L = 295$ km. The characteristic feature of the T2K beam is (apart from its power, that makes this beam a first-generation Super-Beam) that the detector is not on the longitudinal axis of the beam. This feature has a threefold advantage: first, it allows that neutrinos produced through protons whose energy is fixed by the requirement that they may be used for different purposes have a $\nu_\mu \rightarrow \nu_e$ oscillation probability peaked at $L = 295$ km, where the detector is located; second, the off-axis beam is narrower than the on-axis one, thus improving the matching of the L/E ratio with the first peak of the oscillation; third, it allows a reduction of the beam-driven background. Notice that the off-axis angle has not yet been chosen, to arrange the L/E ratio to slight variations in the measured value of Δm_{23}^2 . The technical design of the tunnel is such that the off-axis angle can be modified ranging between 2° and 3° . The T2K fluxes for a 2° off-axis angle as they are expected at the Kamiokande site are shown in Fig. 1(left). Following the Letter of Intent [16], we have considered four 200 MeV bins with $E_{min} = 400$ MeV. The muon and electron identification efficiencies per bin are presented in Fig. 21. The average neutrino energy is $\langle E_\nu \rangle = 0.75$ GeV with 5 years of π^+ running, only.

The dominant background is made of pions from neutral currents. The detector is extremely well understood, being the SuperKamiokande water Čerenkov. As for the SPL,

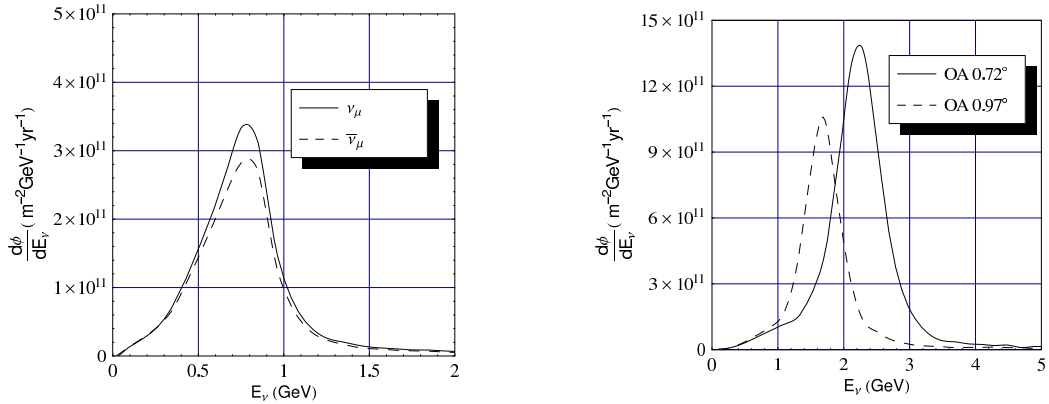


Fig. 1. Left: T2K-I fluxes at the Kamioka location (295 km baseline), [16]; Right: NO ν A fluxes at the far location (812 km baseline), [36].

the dominant sources of systematic error (apart for the neutrino-nucleon cross-sections) are the definition of the fiducial volume in the detector and the overall normalization of the flux. We have introduced a “pessimistic” 5 % global systematic error.

A second phase has been proposed for the T2K experiment: if a positive signal in $\nu_\mu \rightarrow \nu_e$ conversion is observed, the beam power is planned to be increased up to 4 MWatt and the detector mass up to 1 Mton (500 Kt fiducial mass). A 5 years π^+ and 5 years π^- running are envisaged. Such scenario will be called T2K-II in Sect. 5.

2.2 The NO ν A Beam

The NO ν A facility Letter of Intent [24] has passed the first scrutiny. It consists of a conventional beam with 0.7 MWatt power 120 GeV protons produced at the NuMI in FermiLab aiming at a site located at $L = 812$ km from the source. It is still not decided the typology of the detector that will be located there, with two options considered so far: a low- Z calorimeter; or, an Icarus-like liquid argon bubble chamber. As for T2K, the NO ν A detector will be placed at a non-zero off-axis angle with respect to the longitudinal beam direction, to reduce backgrounds and to have a narrow beam to match the L/E oscillation peak ratio. A reduced version of the detector will be placed at the FermiLab site to extrapolate the expected rates and their energy spectrum in the far detector in the absence of oscillation. The NO ν A fluxes for a 0.72° off-axis angle as they are expected at the far site are shown in Fig. 1(right).

In the following, we consider a totally active 30 kton detector made of liquid scintillator and PVC [38] with 6.5×10^{20} pot/y (no proton driver is considered, [37]). The average neutrino energy is $\langle E_\nu \rangle = 2.22$ GeV, with 5 years of π^+ run only [24]. Events are grouped in three ~ 650 MeV bins with $E_{min} = 1000$ MeV, with a constant muon identification efficiency $\epsilon_\mu = 0.9$ [39] and a constant electron identification efficiency $\epsilon_e = 0.24$ [38].

The dominant background for the disappearance channel are $\nu_\mu \rightarrow \nu_x$ neutral currents with a rejection factor at the level of 5×10^{-3} (for the appearance channel the background is typically from electron neutrinos in the beam and from neutral current events faking electron neutrinos, with a rejection factor approximately of 2×10^{-3}).

The main source of systematic errors are the incomplete knowledge of the neutrino flux and the extrapolation of the flux and of the backgrounds from the near to the far detector. The near detector will be used to improve the present knowledge of low energy neutrino cross-sections and to complement the results of the MINER ν A experiment [40] (operating before the bulk of NO ν A data is collected). We have introduced a “pessimistic” 5% global systematic error.

2.3 The SPL

The SPL is a proposal for a high intensity conventional beam with a 4 MWatt 2.2 GeV proton driver located at CERN, Ref. [25]. The neutrino fluxes have first been computed in a full simulation of the beamline in Ref. [41], assuming a decay tunnel length of 60 m. The corresponding fluxes are shown in Fig. 2(left). However, the original beam design was conceived as the first stage of a Neutrino Factory, and it was not optimized as a facility to look for $\nu_\mu \rightarrow \nu_e$ oscillations on its own. Such an optimization has been presented in Ref. [42], and the modified fluxes are shown in Fig. 2(right). We will consider both the “old” and “new” neutrino fluxes to study the potential of the ν_μ disappearance channel at this facility to measure the atmospheric parameters θ_{23} and Δm_{23}^2 .

For both fluxes, a UNO-like [43] 1 Mton water Čerenkov detector (with a 440 kton fiducial volume) located inside the Fréjus tunnel with a baseline $L = 130$ km is considered. The average $\nu_\mu(\bar{\nu}_\mu)$ (anti)neutrino energy for both the “old” and the “new” fluxes is $E_\nu \in [250 - 300]$ MeV, such as to match the first oscillation peak. 2 years of π^+ running and 8 years of π^- running are considered. The detector characteristics when exposed to the SPL beam were studied in detail in Ref. [44], where an almost constant $\epsilon_e = 70$ % efficiency to identify electrons was found. Reasonably enough, due to the low energy of the neutrino flux, no binning was considered (being the neutrino energy comparable with the Fermi motion). Following Ref. [45], however, we try to consider a very coarse binning grouping events in two bins with energies $E_1 \in [0, 250]$ MeV and $E_2 \in [250, 600]$ MeV. We have considered a constant bin independent muon identification efficiency, $\epsilon_{\mu 1} = \epsilon_{\mu 2} = 0.7$. The electron identification efficiency is $\epsilon_{e-} = 0.707, \epsilon_{e+} = 0.671$ [46]. Notice that in the appearance channel no binning is considered, since in the energy range E_1 practically no event is observed.

The background is made dominantly of pions from neutral currents and it is negligible in the range of energy E_2 . The dominant sources of systematic error (apart for the neutrino-nucleon cross-sections) are the definition of the fiducial volume in the detector and the overall normalization of the flux. We have introduced a “pessimistic” 5 % global

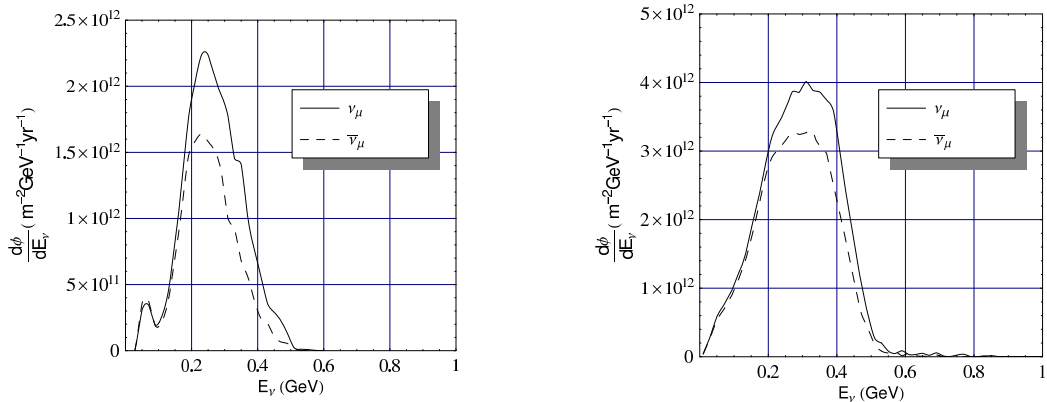


Fig. 2. *Left: Standard SPL Super-Beam fluxes at the Fréjus location (130 km baseline), [41]; Right: Optimized SPL Super-Beam fluxes at the Fréjus location (same baseline) [42].*

systematic error.

2.4 The Neutrino Factory

The Neutrino Factory proposal considered here is a 50 GeV muon storage ring fuelled through a 4 MWatt SPL-like Super-Beam [47], with 2×10^{20} muons decaying in each straight section of the storage ring per year. Five years of data taking for each muon polarity are envisaged. Two detectors of different technology are considered: a 40 kton Magnetized Iron Detector (MID) located at $L = 3000$ km or $L = 7000$ km; and a 10 kton Emulsion Cloud Chamber (ECC) at $L = 732$ km. This proposal corresponds to the design of a possible CERN-based Neutrino Factory Complex, with detectors located at the Gran Sasso Laboratory as the shortest baseline and at a second site to be defined as the medium and long baseline. These detectors have been especially optimized to look for a particular signal: the MID for the “golden” channel $\nu_e \rightarrow \nu_\mu$, and the ECC for the “silver” channel $\nu_e \rightarrow \nu_\tau$. The corresponding neutrino fluxes are shown in Fig. 3(left).

The detectors background, muon identification efficiency and systematics for the golden and silver channels at this specific facility have been studied in Refs. [48] (the Magnetized Iron Detector) and [49] (the Emulsion Cloud Chamber). It has been noticed that the MID simulation must be updated due to the growing evidence for the relevance of low energy bins that were sacrificed at first to reduce backgrounds in Ref. [10]. To take advantage of the low energy bins, in this paper we will consider for the disappearance channel 4 GeV bins when the MID is located at the $L = 3000$ km baseline and 5 GeV bins when the MID is located at the $L = 7000$ km baseline, instead of the 10 GeV bins considered in the appearance channels. The disappearance signal is much different from the golden and silver appearance signals. In particular, not such strong cuts as for the appearance channels signals must be applied to reduce the background. A reasonable constant muon identification efficiency $\epsilon_\mu = 0.7$ has been applied when the

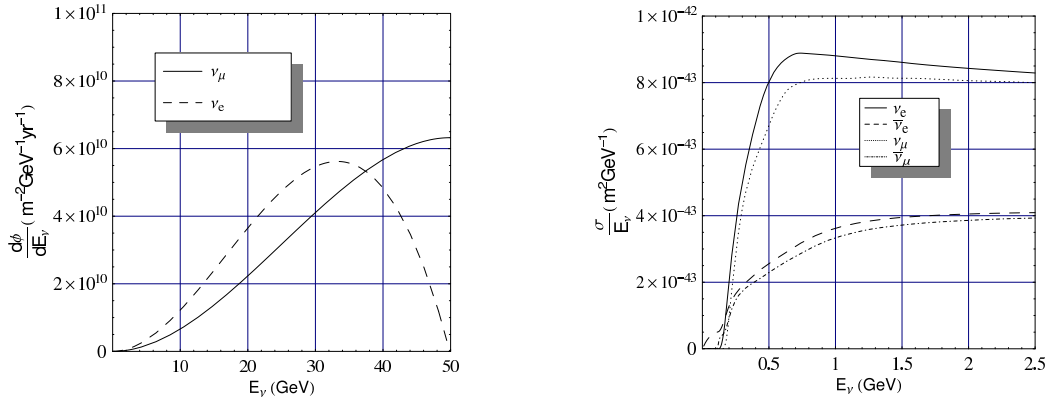


Fig. 3. *Left: 50 GeV Neutrino Factory fluxes at 3000 km [10]; Right: the νN and $\bar{\nu}N$ cross-sections on water [51].*

disappearance channel is considered throughout the paper. A global 2 % systematic error has been included.

2.5 The neutrino cross-section

An important source of systematic error is our present poor knowledge of the νN and $\bar{\nu}N$ cross-sections for energies below 1 GeV [50]: either there are very few data (the case of neutrinos) or there are no data at all (the case of antineutrinos). On top of that, the few available data have generally not been taken on the target used in the experiments (either water, iron, lead or plastics), and the extrapolation from different nuclei is complicated by nuclear effects that at the considered energies can play an important role.

We use for each detector a different cross-section following Ref. [51]. For example, we show in Fig. 3(right) the cross-sections on water used for the water Čerenkov detectors throughout the paper. Notice the difference between the $\nu_e N$ and $\bar{\nu}_e N$ cross-sections: the former, being an interaction between the ν_e and a neutron inside the oxygen nucleus, is affected by nuclear effects and thus shows a threshold energy. The latter is mainly a $\bar{\nu}_e$ interaction with the protons of the two hydrogens, approximately free. This effect, although less pronounced, is visible also for ν_μ and for $\bar{\nu}_\mu$. This feature is quite relevant for neutrino/antineutrino of hundreds of MeV energy, region where different cross-sections can easily differ by a factor 2. Be aware that there are other nuclear effects (see Ref. [52] and references therein) not included yet in any of the available calculations that could play an important effect at the cross-section threshold energy.

In the rest of the paper, we will make use of cross-sections on iron, lead and scintillator for the MID, the ECC and the NOVA detectors, respectively.

3 The measurement of θ_{23} and Δm_{23}^2 at SPL, T2K and NO ν A.

3.1 Correlations and degeneracies in ν_μ disappearance

A conventional beam with ν_μ neutrinos of moderate energy can perform an independent measurement of the atmospheric parameters θ_{23} and Δm_{23}^2 via the ν_μ disappearance channel: it is expected that this kind of facilities will reduce the error on the atmospheric mass difference to less than 10 % in a few years for $\Delta m_{23}^2 \geq 2.2 \times 10^{-3} \text{ eV}^2$ [53]. The expected error on the atmospheric angle depends on the value of θ_{23} itself, the smallest error for large but non maximal mixing (as it has been shown in Ref. [54]). It is interesting to study in detail the parameter correlations and degeneracies that affect this measurement and that can induce large errors. We remind the vacuum oscillation probability expanded to the second order in the small parameters θ_{13} and $(\Delta_{12}L/E)$ [55]:

$$\begin{aligned}
P(\nu_\mu \rightarrow \nu_\mu) = & 1 - \left[\sin^2 2\theta_{23} - s_{23}^2 \sin^2 2\theta_{13} \cos 2\theta_{23} \right] \sin^2 \left(\frac{\Delta_{23}L}{2} \right) \\
& - \left(\frac{\Delta_{12}L}{2} \right) [s_{12}^2 \sin^2 2\theta_{23} + \tilde{J}s_{23}^2 \cos \delta] \sin(\Delta_{23}L) \\
& - \left(\frac{\Delta_{12}L}{2} \right)^2 [c_{23}^4 \sin^2 2\theta_{12} + s_{12}^2 \sin^2 2\theta_{23} \cos(\Delta_{23}L)]
\end{aligned} \tag{1}$$

where $\tilde{J} = \cos \theta_{13} \sin 2\theta_{12} \sin 2\theta_{13} \sin 2\theta_{23}$ and $\Delta_{23} = \Delta m_{23}^2/2E$, $\Delta_{12} = \Delta m_{12}^2/2E$. The first term in the first parenthesis is the dominant one and is symmetric under $\theta_{23} \rightarrow \pi/2 - \theta_{23}$. This is indeed the source of our present ignorance on the θ_{23} -octant [13], parametrized by $s_{oct} = \text{sign}(\tan 2\theta_{23})$. This symmetry is lifted by the other terms, that introduce a mild CP-conserving δ -dependence also, albeit through subleading effects very difficult to isolate.

Considering that the sign of the atmospheric mass difference, $s_{atm} = \text{sign}(\Delta m_{23}^2)$, is unknown at present, for any experimental input $(\bar{\theta}_{23}, \Delta m_{atm}^2)$ we must solve two systems of equations:

$$N_{\mu\mu}^\pm(\bar{\theta}_{23}, \Delta m_{atm}^2; \bar{s}_{atm}) = N_{\mu\mu}^\pm(\theta_{23}, |\Delta m_{23}^2|; \bar{s}_{atm}), \tag{2}$$

$$N_{\mu\mu}^\pm(\bar{\theta}_{23}, \Delta m_{atm}^2; \bar{s}_{atm}) = N_{\mu\mu}^\pm(\theta_{23}, |\Delta m_{23}^2|; -\bar{s}_{atm}), \tag{3}$$

where \bar{s}_{atm} is the physical mass hierarchy.

For non maximal $\bar{\theta}_{23}$ four different solutions are found: for $|\Delta m_{23}^2| \sim \Delta m_{atm}^2$ we get two solutions from eq. (2), i.e. the input value $\theta_{23} = \bar{\theta}_{23}$ and $\theta_{23} \simeq \pi/2 - \bar{\theta}_{23}$, being the second solution not exactly at $\theta_{23} = \pi/2 - \bar{\theta}_{23}$ due to the small θ_{23} -octant asymmetry; and two more solutions from eq. (3) at a different value of $|\Delta m_{23}^2|$ [20]. In eq. (1) we can see that changing sign to Δm_{23}^2 the second term becomes positive: a change

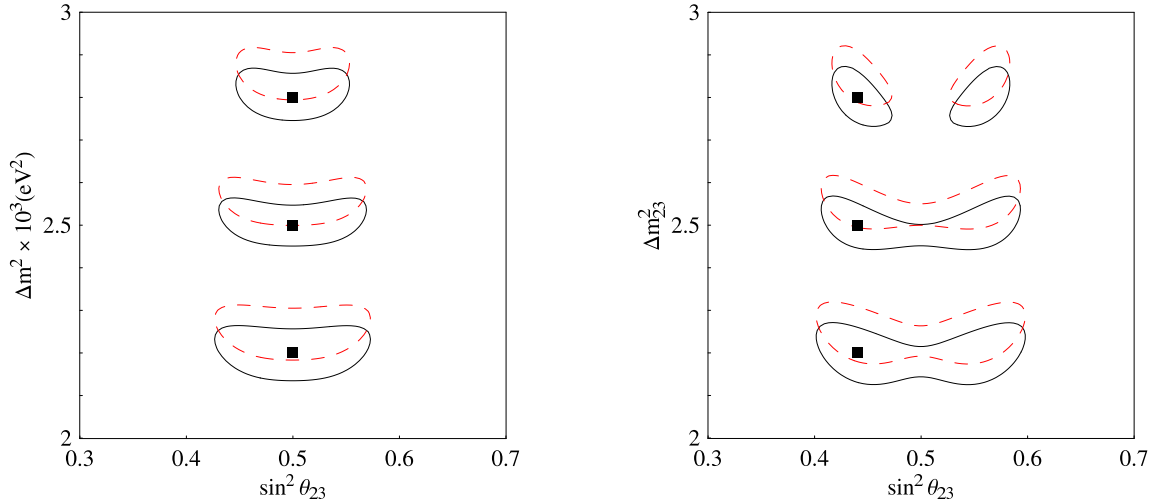


Fig. 4. *The sign degeneracy at T2K-I; left: $\theta_{23} = 45^\circ$; right: $\theta_{23} = 41.5^\circ$.*

that must be compensated with an increase in $|\Delta m_{23}^2|$ to give $P_{\mu\mu}^\pm(\Delta m_{atm}^2; \bar{s}_{atm}) = P_{\mu\mu}^\pm(|\Delta m_{23}^2|; -\bar{s}_{atm})$.

The result of a fit to the disappearance channel data at the T2K-phase I experiment is depicted in Fig. 4 for three different values of the atmospheric mass difference: $\Delta m_{23}^2 = (2.2, 2.5, 2.8) \times 10^{-3} \text{ eV}^2$. Fixed values of the solar parameters have been used, $\Delta m_{12}^2 = 8.2 \times 10^{-5} \text{ eV}^2$; $\theta_{12} = 33^\circ$. For maximal atmospheric mixing $\theta_{23} = 45^\circ$, Fig. 4 (left), two solutions are found at 90 % CL when both choices of s_{atm} are considered. On the other hand, using a non maximal input atmospheric angle $\theta_{23} = 41.5^\circ$ ($\sin^2 \theta_{23} = 0.44$) [6] four degenerate solutions are found, Fig. 4(right). In general, we must therefore speak of a two-fold or four-fold degeneracy in the disappearance channel, as it was pointed out in Ref. [20].

Notice how the *disappearance sign clones* appears at a value of $|\Delta m_{23}^2|$ higher than the input value, as it was expected from eq. (1). The shift in the vertical axis is a function of θ_{13} and δ , that in this particular case have been kept fixed to $\theta_{13} = 0^\circ = \delta$. The degeneracy can be softened or solved by using detectors with large baselines that can exploit matter effects, as it will be shown in Sect. 4. Notice, eventually, that the uncertainty on the atmospheric parameters can be enhanced once we take into account that θ_{13} and δ are unknown [54]. This will be studied in Sect. 3.4.

3.2 A matter of conventions

It is useful to open here a short parenthesis to address a problem that arised recently concerning the “physical” meaning of the variable used to fit the “atmospheric” mass difference, Δm_{atm}^2 . Notice, first of all, that the experimentally measured solar mass difference Δm_{sol}^2 can be unambiguously identified with the three-family parameter $\Delta m_{12}^2 = m_2^2 - m_1^2$. This is not true for the experimentally measured atmospheric mass difference Δm_{atm}^2 . Since the subleading solar effects are, at present, barely seen in

atmospheric neutrino experiments, we can define in different ways the three-family parameter to be used in the fits: for example, using $\Delta m_{23}^2 = m_3^2 - m_2^2$ (the choice adopted throughout this paper), or $\Delta m_{13}^2 = m_3^2 - m_1^2$, or even $\Delta m^2 = (\Delta m_{23}^2 + \Delta m_{13}^2)/2$, [56], we will get in general the same results using present data. When future experiments aiming to the measurement of the atmospheric mass difference at the level of 10^{-4} eV² will be running, however, different choices of the fitting parameter will give different results.

This can be observed in Fig. 5, where the three choices introduced above are compared. We plot in the three panels the 90 % CL contours resulting from a fit to the experimental data corresponding to the input value, $\Delta m_{atm}^2 = 2.5 \times 10^{-3}$, in normal hierarchy, but fitted in turn in Δm_{23}^2 (left panel), Δm_{13}^2 (middle panel) and Δm^2 (right panel). As it can be seen in the figure, the contour corresponding to the normal hierarchy, $s_{atm} = \bar{s}_{atm}$, is always located around the input value (in each plot the input value corresponds to a different fitting variable, though). On the other hand, the contour obtained for the inverted hierarchy is located above, below and on top of the input value, respectively, depending on the fitting variable. This is a clear consequence of the fact that the difference between each of the possible choices is $O(\Delta m_{12}^2)$ and it is reflected in a different form of eq. (1).

Up to here, it is perfectly clear what happens whenever we use a certain three-family variable to fit the results that at present are given under the label Δm_{atm}^2 . A philosophical discussion, however, arised around the “physical” meaning of the different choices reported above. The idea is that the “physically meaningful” quantities to be measured in oscillation experiments are the “oscillation frequencies”. For three-family mixing, three “frequencies” can be defined, the shortest being the solar oscillation frequency (as we said, unambiguously related to the mass difference Δm_{12}^2). In normal hierarchy, the middle frequency is related to Δm_{23}^2 and the longest one to Δm_{13}^2 . In inverted hierarchy these two frequencies are interchanged and the middle frequency will be related to Δm_{31}^2 and not to Δm_{32}^2 . For this reason, it has been suggested that plots in different hierarchies should be presented using different variables where maintaining the ordering of the oscillation frequencies. For example, if we choose to identify Δm_{atm}^2 with Δm_{23}^2 in normal hierarchy (i.e., with the middle frequency), we should identify it with Δm_{31}^2 in inverted hierarchy (i.e., again with the middle frequency). As a consequence, we could not plot contours for the two hierarchies on the same figure (the vertical axis corresponds to different variables depending on the choice of s_{atm}). This is a drawback of giving to the oscillation frequencies a deeper physical meaning than to the mass differences. A new variable to be identified with Δm_{atm}^2 has been introduced in Ref. [56]: $\Delta m^2 = (\Delta m_{23}^2 + \Delta m_{13}^2)/2$. When changing hierarchy, this variable just flip its sign (since $\Delta m_{23}^2 \rightarrow -\Delta m_{13}^2$ and viceversa). It is thus possible to present both hierarchies in the same figure with $|\Delta m^2|$ in the vertical axis. The oscillation frequency related to this variable is neither the longest nor the middle one, but it maintains its role of next-to-longest or a-bit-longer-than-the-middle-one in both hierarchies⁴.

⁴ It should be stressed that even fitting in inverted hierarchy using Δm^2 as the fitting vari-

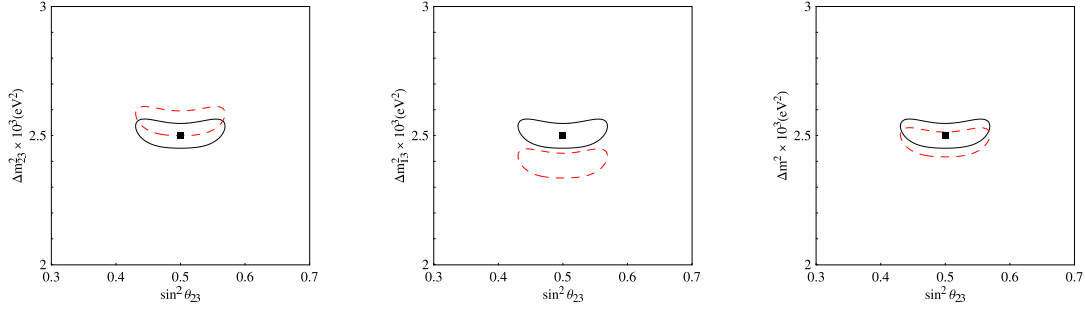


Fig. 5. *Different choices of the three-family “atmospheric” mass difference; left: Δm_{23}^2 ; middle: Δm_{13}^2 ; right: Δm^2 , [56].*

It seems to us that the “physical meaning” of a frequency is not deeper than that of a mass difference, and that it is perfectly acceptable to use any variable to fit the experimental data when considering a full three-family analysis. What is really important is to be consistent with the adopted choice, in particular when adding appearance and disappearance data, something that we will do in Sect. 3.4. In the rest of the paper we adopt Δm_{23}^2 as fitting variable.

3.3 The importance of energy resolution

It is extremely important that an experiment whose goal is to improve significantly the present uncertainties on the atmospheric parameters may be able to use energy dependence. A counting experiment is certainly limited, as it has been shown in Refs. [57,20].

In Fig. 6 we present a comparison of the disappearance channel at T2K-phase I (left panels) and NO ν A (right panels). Both maximal mixing, $\theta_{23} = 45^\circ$ (top panels), and non maximal mixing, $\theta_{23} = 41.5^\circ$ (bottom panels), are used as input values. In each plot we present the 90% CL contours in the $(\theta_{23}, \Delta m_{23}^2)$ plane for different energy bins (only the bins corresponding to neutrinos with energy just below and above the peak energy are reported for T2K, all bins for NO ν A). Again, solar parameters are kept fixed to their present best fit values, $\Delta m_{12}^2 = 8.2 \times 10^{-5} \text{ eV}^2$, $\theta_{12} = 33^\circ$, and the unknowns are fixed to $\theta_{13} = \delta = 0^\circ$. Both for T2K-phase I and NO ν A 5 years of π^+ are considered. Notice that the contours corresponding to neutrinos with an energy below and above the oscillation peak have a different shape. As a consequence, the combination of different bins significantly increases the θ_{23} resolution of the experiment with respect to a counting experiment. It can be seen that T2K-I is able to measure Δm_{23}^2 with a precision of less than 10^{-4} eV^2 for $\Delta m_{23}^2 = 2.5 \times 10^{-3} \text{ eV}^2$. However, it is not able to exclude maximal mixing at 90 % CL for $\theta_{23} = 41.5^\circ$. The same happens for NO ν A, see Fig. 6(right).

In Fig. 7 we present a comparison of the disappearance channel at the SPL using the neutrino fluxes of Ref. [41], Fig. 2(left panels), or the neutrino fluxes of Ref. [42],

able, the allowed region is shifted with respect to that corresponding to the normal hierarchy. This can be observed in Fig. 5(right), and it implies that $|\Delta m^2|_{NH} \neq |\Delta m^2|_{IH}$.

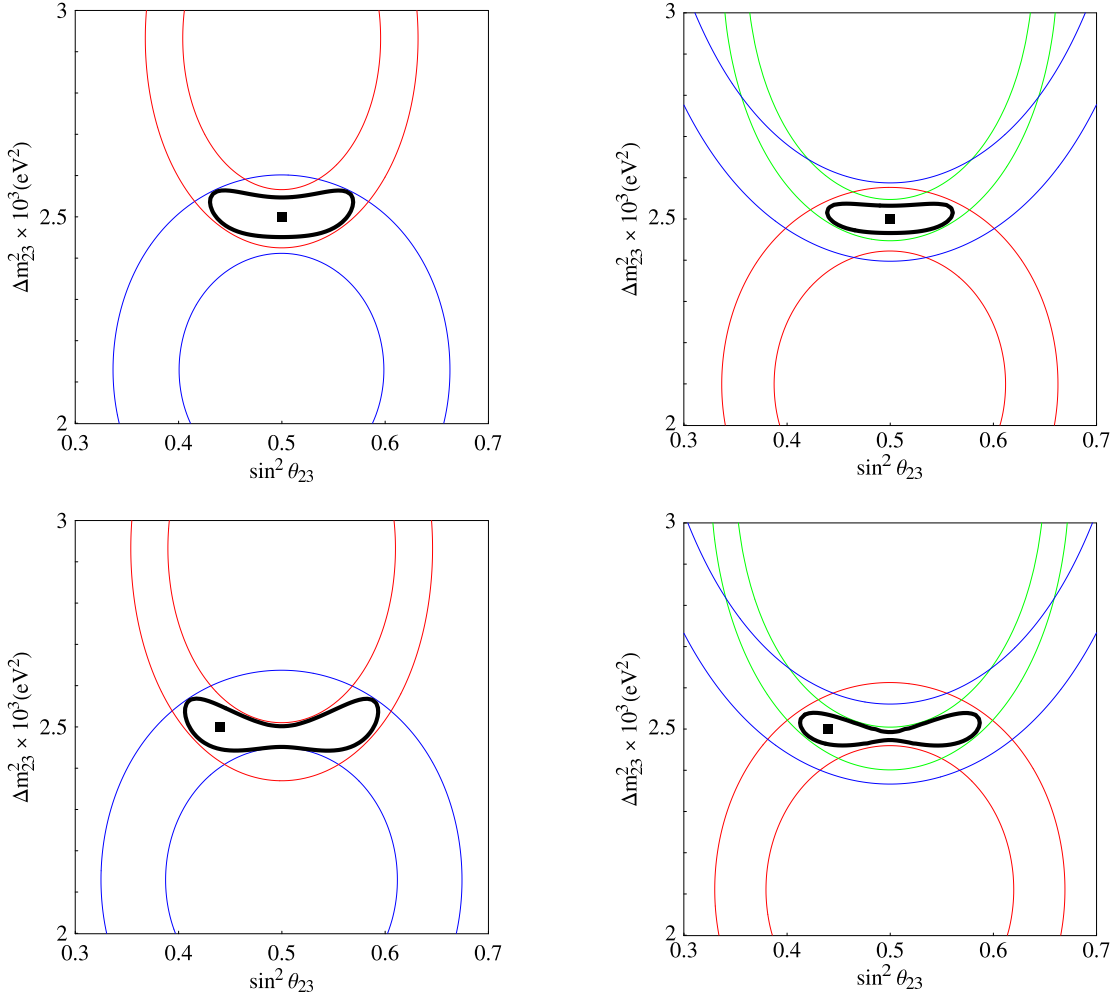


Fig. 6. *Binning at T2K-I (left) and NOνA (right); top: $\theta_{23} = 45^\circ$; bottom: $\theta_{23} = 41.5^\circ$.*

Fig. 2(right panels), again for both maximal mixing, $\theta_{23} = 45^\circ$ (top panels), and non maximal mixing, $\theta_{23} = 41.5^\circ$ (bottom panels). The 90 % CL contours corresponding to both SPL energy bins are drawn. In this case, both neutrinos and antineutrinos fluxes are produced by π^+ and π^- decays with 2 and 8 years of data taking, respectively. Notice that, however, being the neutrino and antineutrino average energies extremely similar in this setup, the neutrino (antineutrino) contours are almost superimposed. As a consequence, experimental information from the neutrino and the antineutrino fluxes is not complementary and we observe just an increase in the statistics. For this reason, although in this setup a 1 Mton detector is considered, the resolution in θ_{23} is not astonishing. A big improvement with respect to the results presented for this facility in Ref. [20,15] is represented by the spectral information: in the new analysis two energy bins are considered for both setups. Thanks to this, maximal mixing can be excluded at 90 % CL for $\theta_{23} = 41.5^\circ$. As a final comment, notice that the new neutrino fluxes of Ref. [42] do not improve the θ_{23} resolution with respect to old fluxes from Ref. [41]. This is because the new fluxes have been optimized to look for the $\nu_\mu \rightarrow \nu_e$ appearance

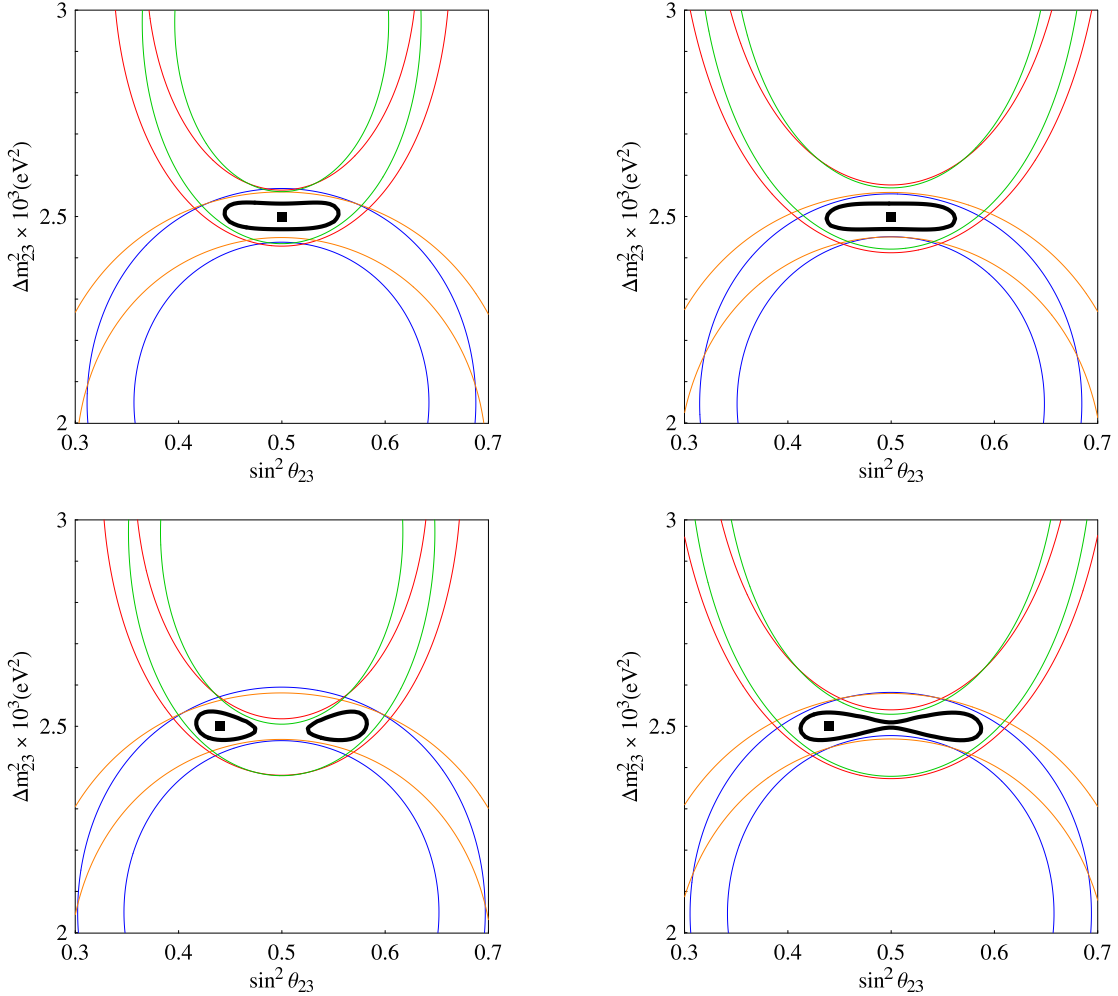


Fig. 7. *Binning at the standard (left) and optimized SPL (right); top: $\theta_{23} = 45^\circ$; bottom: $\theta_{23} = 41.5^\circ$.*

signal and not to the $\nu_\mu \rightarrow \nu_\mu$ disappearance one. In particular, the average neutrino and antineutrino energies are identical (see Fig. 2) and thus the small complementarity of the two fluxes reduces. In the rest of the paper we will consider the SPL with old fluxes, only.

It is remarkable how a relatively “small” experiment such as T2K-I, with only 5 years of data taking in one polarity and with a 22.5 Kton water Čerenkov detector, has a resolution in Δm_{23}^2 and θ_{23} not much worse than the SPL facility, with a much larger 1 Mton water Čerenkov and 10 years of data taking in both pion polarities (compare the left panels of Figs. 6 and 7). One of the reasons is that the SPL has both neutrino and antineutrino beams with an average energy corresponding to the oscillation peak for the $L = 130$ baseline. As a consequence, information coming from the two beams just add statistically but it is not complementary (in the absence of matter effects). It would be better to run the SPL with neutrinos again but at a different energy (not at the oscillation peak) after the first two years with π^+ .

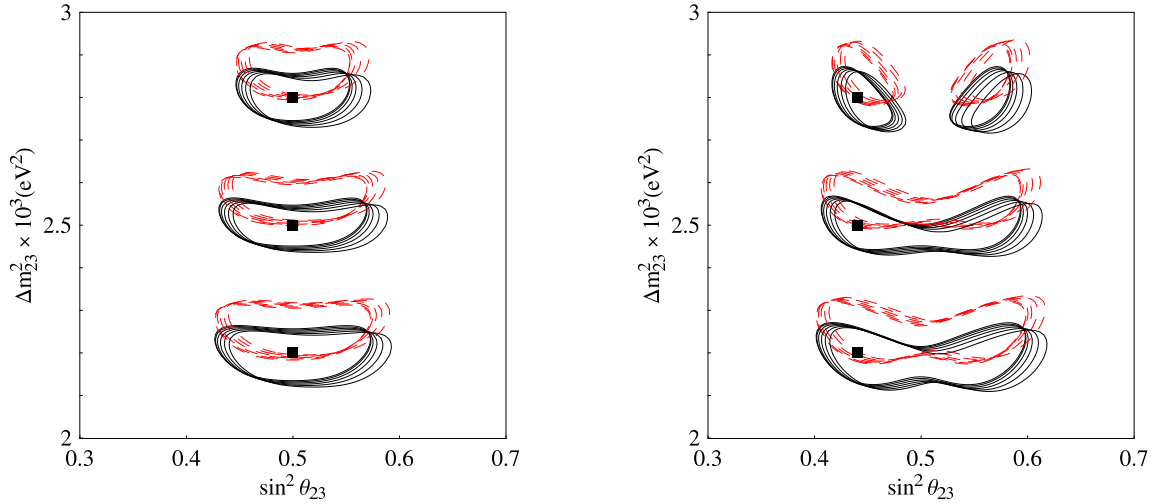


Fig. 8. The impact of θ_{13} at T2K-I; left: $\theta_{23} = 45^\circ$; right: $\theta_{23} = 41.5^\circ$.

3.4 The impact of θ_{13} and δ

Up to this moment we have kept the unknown parameters θ_{13} and δ as external fixed quantities, $\theta_{13} = \delta = 0^\circ$, following what we have done for the solar parameters Δm_{12}^2 and θ_{12} . However, the two sets of parameters should be treated differently. Indeed, we do have a good measure of solar parameters and it has been shown in the literature that the impact of solar parameter uncertainties in the measurement of atmospheric parameters is negligible [15]. The main effect is the shift in the atmospheric mass difference fitting variable, as it has been discussed in Sect. 3.2. This is not the case for the unknown parameters (θ_{13}, δ) . Being both parameters unknown, we must fit the atmospheric parameters introducing them as free variables to be reconstructed at the same time with $(\theta_{23}, \Delta m_{23}^2)$. A recent comprehensive three-families analysis of present solar, atmospheric and reactor data can be found, for example, in Ref. [6].

In Fig. 8 we show the effect of a varying θ_{13} (but fixed δ) on the previous fits at T2K-I for $\theta_{23} = 45^\circ$ (left panel) and $\theta_{23} = 41.5^\circ$ (right panel) and three values of the atmospheric mass difference, $\Delta m_{23}^2 = (2.2, 2.5, 2.8) \times 10^{-3} \text{ eV}^2$. Both choices of s_{atm} are shown on the same plot. The input values of the unknowns are: $\bar{\theta}_{13} = 0^\circ$, $\bar{\delta} = 0^\circ$. In the fit, θ_{13} is free to vary in the range $\theta_{13} \in [0^\circ, 10^\circ]$. Notice that the input values can be fitted with increasing values of θ_{13} if θ_{23} is also increased, resulting in a shift of the 90 % CL contours to the right. This is a consequence of the θ_{23} -asymmetric second term in the first parenthesis of eq. (1).

Such a naive treatment of the experimental data is, however, not correct. The considered Super-Beam facilities have indeed been proposed to look for the appearance $\nu_\mu \rightarrow \nu_e$ channel, the oscillation probability in vacuum expanded to the second order in the small parameters θ_{13} and $(\Delta_{12}L/E)$ [10,55] for which is:

$$P^\pm(\nu_\mu \rightarrow \nu_e) = s_{23}^2 \sin^2(2\theta_{13}) \sin^2\left(\frac{\Delta_{23}L}{2}\right) \quad (4)$$

$$\begin{aligned}
& + \sin(2\theta_{12}) \sin(2\theta_{23}) \sin(2\theta_{13}) \cos\left(\mp\delta - \frac{\Delta_{23}L}{2}\right) \sin\left(\frac{\Delta_{12}L}{2}\right) \sin\left(\frac{\Delta_{23}L}{2}\right) \\
& + c_{23}^2 \sin^2(2\theta_{12}) \sin^2\left(\frac{\Delta_{12}L}{2}\right),
\end{aligned}$$

where \pm refers to neutrinos and antineutrinos, respectively. It is clear that to take properly into account the effect of (θ_{13}, δ) we should combine (whenever possible) appearance and disappearance signals at a given facility.

The results of a four-parameters fit in $(\theta_{23}, \Delta m_{23}^2, \theta_{13}, \delta)$ projected onto the $(\theta_{23}, \Delta m_{23}^2)$ plane obtained by combining the disappearance and appearance signals at the T2K-I, NO ν A and SPL facilities are presented in Figs. 9-11, respectively. In all figures two choices of $\bar{\theta}_{23}$ and $\bar{\theta}_{13}$ are shown, $\bar{\theta}_{23} = 45^\circ, 41.5^\circ$ (left and right panels) and $\bar{\theta}_{13} = 0^\circ, 8^\circ$ (top and bottom panels), whereas $\bar{\delta} = 0^\circ$. Solid lines represent the result of a fit with variable θ_{13} and δ . As a reference, we also present the results of a fit⁵ with $\theta_{13} = \bar{\theta}_{13}$ and $\delta = \bar{\delta}$ (dotted lines). It can be observed that in most of the cases the combination of disappearance with appearance signals reduces the spread in θ_{23} that was observed in Fig. 8. Only for $\bar{\theta}_{13}$ large we can still see some effect.

Eventually, the effect of a non-vanishing $\bar{\delta}$ can be easily understood: the CP-conserving δ -dependent term in the second row of eq. (1) is positive for $|\bar{\delta}| \in [0^\circ, 90^\circ]$, negative for $|\bar{\delta}| \in [90^\circ, 180^\circ]$ and vanishing for $|\bar{\delta}| = 90^\circ$. When non-vanishing, this term induces a shift in the fitted value of Δm_{23}^2 that is maximal (minimal) for $\bar{\delta} = 0^\circ$ ($\bar{\delta} = 180^\circ$). Being, however, a θ_{13} -suppressed perturbation on the subdominant $O(\Delta m_{12}^2)$ term, its effect is rather small and it will not be shown in a separate figure.

As a final comment, we notice that the three considered Super-Beams are indeed capable of strongly reducing the present uncertainties on the atmospheric parameters θ_{23} and Δm_{23}^2 , in particular for large values of θ_{13} when combination of appearance and disappearance signals is most effective. For $\theta_{13} = 8^\circ$, for example, maximal atmospheric mixing can be excluded at 90 % CL at all three facilities for $\bar{\theta}_{23} = 41.5^\circ$ (only the SPL, with its gigantic 1 Mton water Čerenkov, is able to exclude maximal mixing for $\bar{\theta}_{23} = 41.5^\circ$ for a vanishing θ_{13}). Notice, however, that while the *disappearance octant degeneracy* appears to be solved when combining disappearance and appearance signals for $\bar{\theta}_{13} = 8^\circ$ when θ_{13} is treated as a fixed parameter, is indeed restored if θ_{13} is left freely varying in the presently allowed range.

4 Appearance and disappearance channels at the Neutrino Factory.

The disappearance signal has not yet been deeply investigated in the framework of the Neutrino Factory (see, however, Ref. [27]). The top-charted signals have been up to now the “golden” $\nu_e \rightarrow \nu_\mu$ [10] and the “silver” $\nu_e \rightarrow \nu_\tau$ [28] channels. However, the Neutrino Factory produces a very intense ν_μ beam that can be used to measure $\nu_\mu \rightarrow \nu_\mu$ and the

⁵ Only the results for $s_{atm} = \bar{s}_{atm}$ are shown.

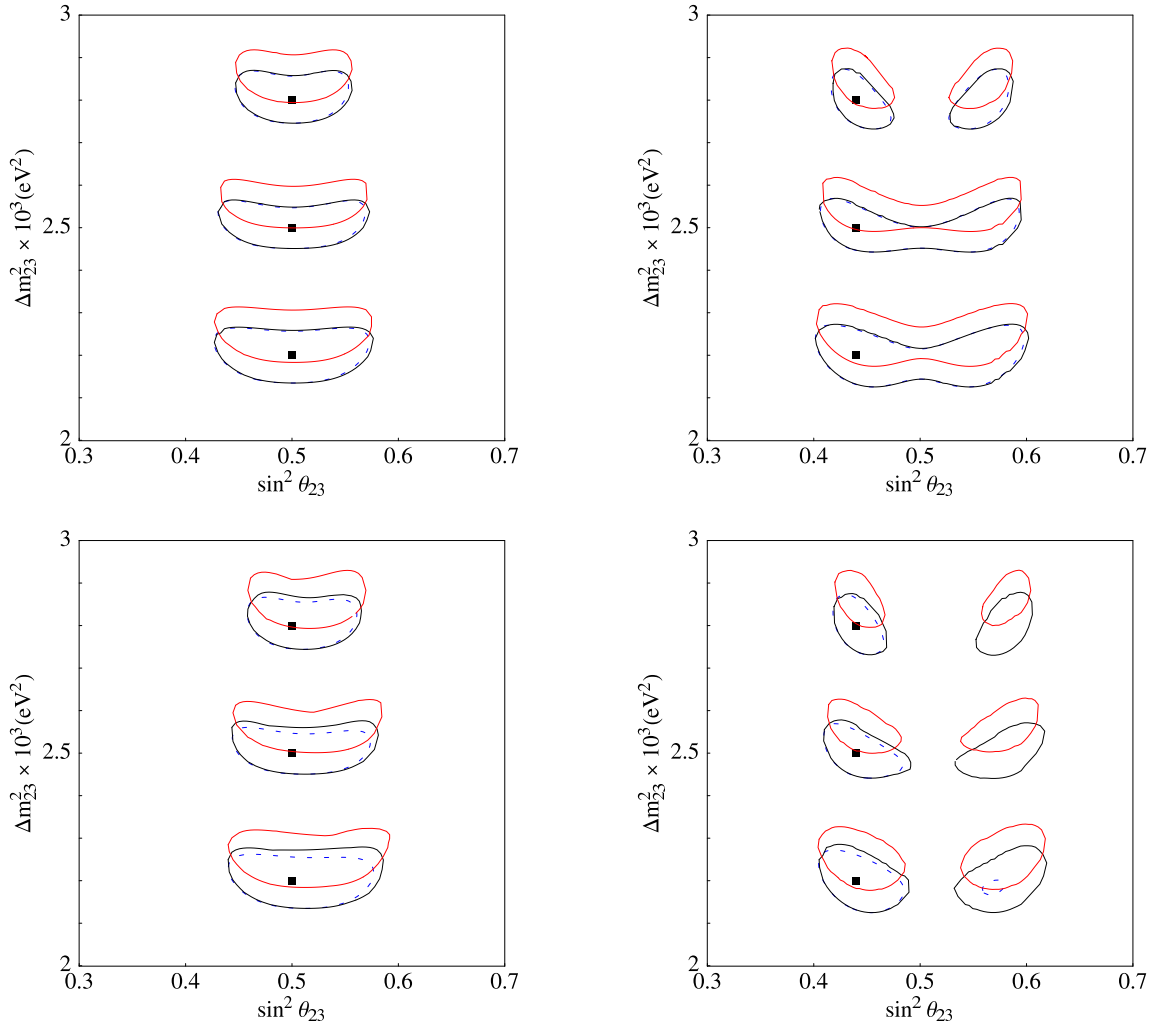


Fig. 9. *Appearance and disappearance at T2K-I. Left: $\theta_{23} = 45^\circ$; right: $\theta_{23} = 41.5^\circ$; top: $\theta_{13} = 0^\circ$; bottom: $\theta_{13} = 8^\circ$.*

leading $\nu_\mu \rightarrow \nu_\tau$ appearance channel as well. This last transition is probably the best signal to improve significantly the atmospheric parameter uncertainties. However, to study it in detail we need a detector able to identify efficiently an enormous amount of τ 's (roughly 1000 and 400 τ^- and τ^+ are expected, respectively), such as it is expected in a Neutrino Factory beam. This detector can be in principle the same used to look for the silver channel, but the needed scaling of the scanning power must be carefully studied and it will not be discussed here. We will devote this Section to a detailed study of the combination of golden, silver and disappearance channels at the Neutrino Factory.

Two possible baselines are studied, $L = 3000$ km and $L = 7000$ km, i.e. the optimal distance to look for a CP-violating signal [10] and the optimal distance to exploit matter effects through the disappearance channel, respectively.

In Figs. 12 and 13 we first present the 90 % contours of the on-peak and above-peak

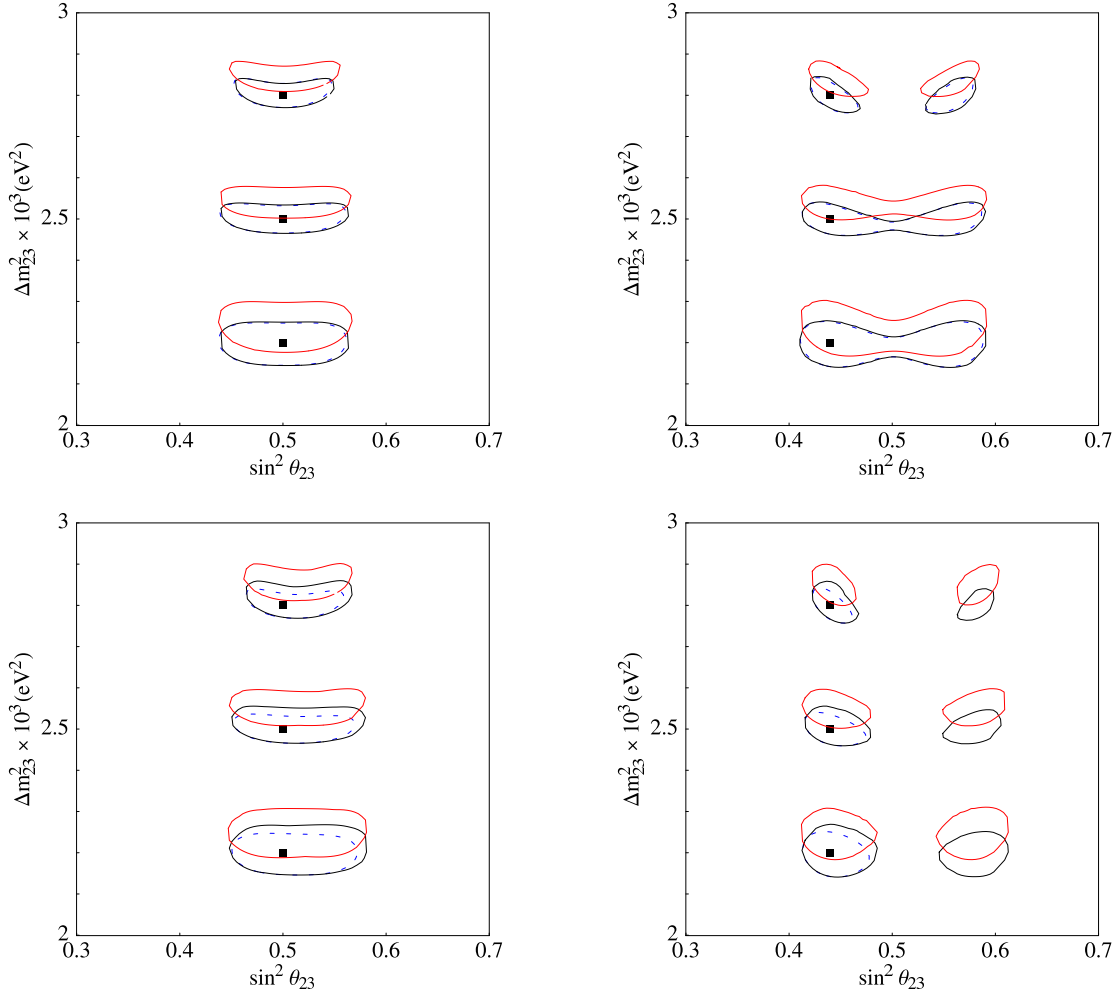


Fig. 10. *Appearance and disappearance at NOνA. Left: $\theta_{23} = 45^\circ$; right: $\theta_{23} = 41.5^\circ$; top: $\theta_{13} = 0^\circ$; bottom: $\theta_{13} = 8^\circ$.*

disappearance channel energy bins for two values of θ_{23} , $\bar{\theta}_{23} = 41.5^\circ, 45^\circ$ (left and right panels, respectively), and two values of θ_{13} , $\bar{\theta}_{13} = 0^\circ, 8^\circ$ (top and bottom panels, respectively). The medium baseline results are shown in Fig. 12, the long baseline results in Fig. 13. Both neutrino and antineutrino bins are presented. Again, solar parameters are kept fixed to their present best fit values, $\Delta m_{12}^2 = 8.2 \times 10^{-5} \text{ eV}^2$, $\theta_{12} = 33^\circ$. The input value for δ is $\bar{\delta} = 0^\circ$.

Notice, first of all, that the resolution in θ_{23} is extremely good and that maximal mixing can be easily excluded for $\theta_{23} = 41.5^\circ$. In particular, at the $L = 7000$ baseline a 4 % error on θ_{23} for $\theta_{23} = 41.5^\circ$ is found. This was expected, being the statistics much higher than at the Super-Beams experiments studied in Sect. 3 (see Tabs. 1-5). Moreover, a new feature arises for $\theta_{13} = 8^\circ$ at both baselines. When a rather large non-vanishing θ_{13} is switched on, matter effects become extremely important and introduce a strong θ_{23} -asymmetry in eq. (1). The asymmetry can be clearly seen in the bottom panels of Figs. 12 and 13, and it is crucial in solving the *disappearance octant degeneracy*, see

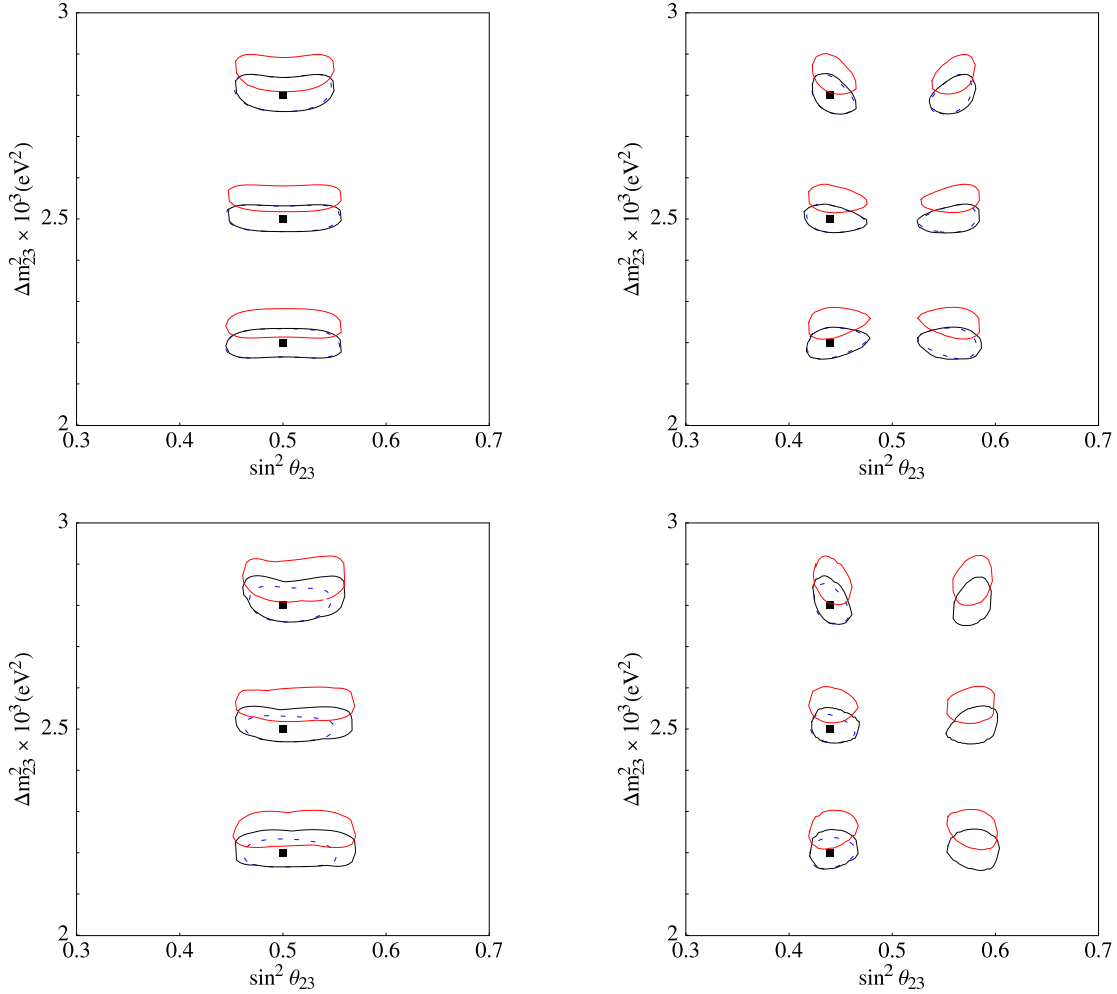


Fig. 11. *Appearance and disappearance at the standard SPL. Left: $\theta_{23} = 45^\circ$; right: $\theta_{23} = 41.5^\circ$; top: $\theta_{13} = 0^\circ$; bottom: $\theta_{13} = 8^\circ$.*

Sect. 3.1.

We point out that the on-peak bin shows a circular shape centered around the input value, distinct from the upward(downward)-curved shapes of contours corresponding to above(below)-peak bins of Figs. 6 and 7. This is because the Neutrino Factory flux is not centered around the peak energy for the chosen baselines: the peak energy for a $L = 3000$ km baseline would be $\langle E_{\nu_\mu} \rangle \sim 6$ GeV and for a $L = 7000$ km baseline $\langle E_{\nu_\mu} \rangle \sim 14$ GeV. As a consequence, we have no energy bins below the peak energy, but only on-peak or above-peak bins. This is a major flaw of the present Neutrino Factory design, that could perhaps be solved with an improved detector capable to take advantage of low energy bins.

The solving of the octant-degeneracy in the disappearance channel (for large θ_{13}) is of great importance. It is useful to recall that, when looking for a CP-violating signal in appearance channels as $\nu_e \rightarrow \nu_\mu, \nu_e \rightarrow \nu_\tau$ and $\nu_\mu \rightarrow \nu_e$, we must deal in general with an eightfold-degeneracy [14] that originates from three sources: the discrete ambiguities

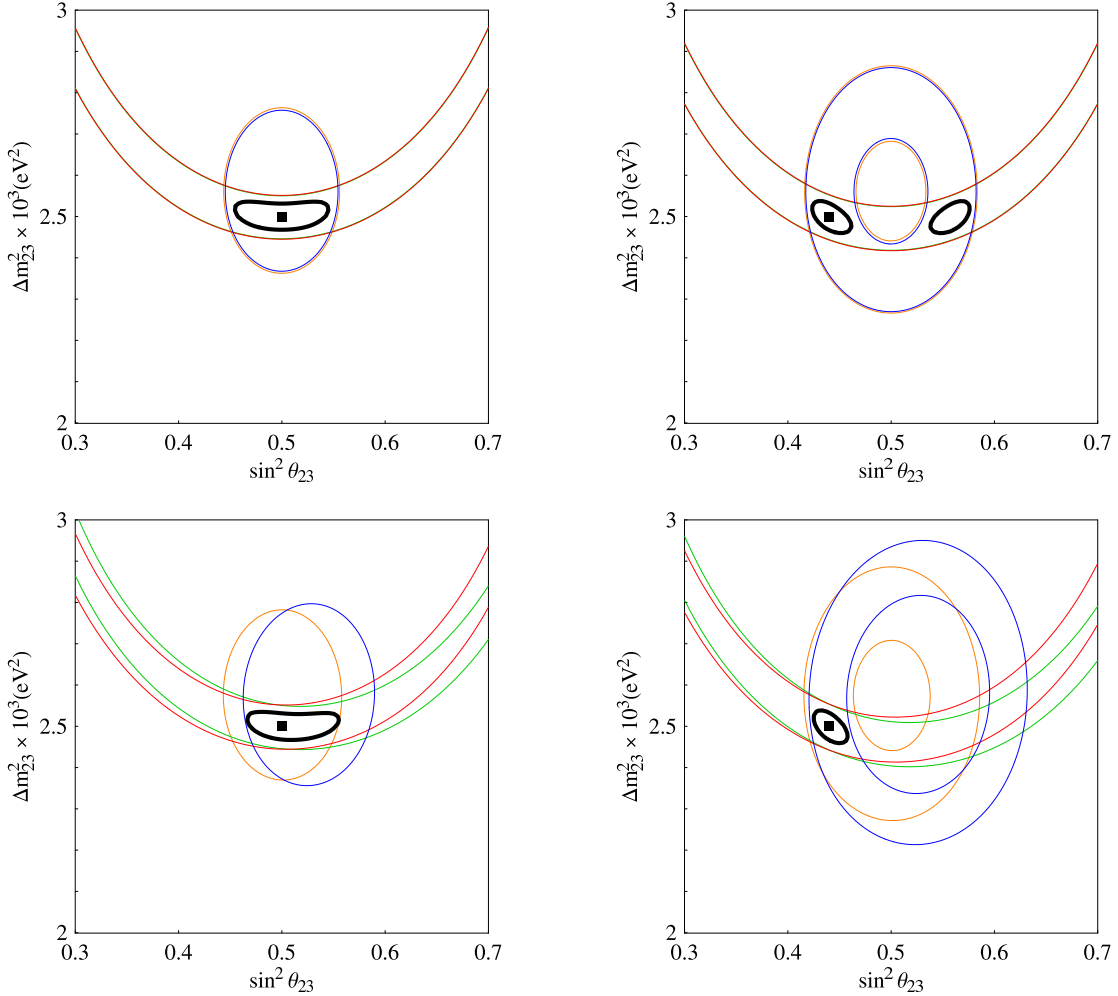


Fig. 12. *Binning at the $L = 3000$ km Neutrino Factory. Left: $\theta_{23} = 45^\circ$; right: $\theta_{23} = 41.5^\circ$; top: $\theta_{13} = 0^\circ$; bottom: $\theta_{13} = 8^\circ$.*

parametrized by s_{atm} [12] and s_{oct} [13] and the *intrinsic* ambiguity due to the trigonometric nature of $P_{e\mu}$, $P_{e\tau}$ and $P_{\mu e}$ in the two unknowns θ_{13} and δ [11] (see eq. (4) as an example). As a consequence, for generic values of the input pair $(\bar{\theta}_{13}, \bar{\delta})$, we get eight different solutions in the (θ_{13}, δ) plane. Different ways to solve the eightfold ambiguity have been proposed in the literature, such as to combine experiments with different L/E [11], or the golden channel at the Neutrino Factory with $\nu_\mu \rightarrow \nu_e$ at a Super-Beam [31], or the golden and silver channels at the Neutrino Factory [28,49], or even to combine different SuperBeams [58,59] or a SuperBeam and a β -Beam [60,57] (see also Refs. [61]-[65]). In Ref. [66] it was shown that the combination of the Neutrino Factory with a SPL-like SuperBeam was able to solve the eightfold-degeneracy and to give a single allowed region in the (θ_{13}, δ) plane at the price of three specialized detectors, a 40 kton Magnetized Iron Calorimeter and a 4 kton Emulsion Cloud Chamber (to look for $\nu_e \rightarrow \nu_\mu$ and $\nu_e \rightarrow \nu_\tau$ oscillations, respectively) and a gigantic 1 Mton Water Čerenkov (to look for $\nu_\mu \rightarrow \nu_e$). The results of Figs. 12 and 13 suggest, on the other hand, that some reduction of the eightfold ambiguity can be achieved at the Neutrino

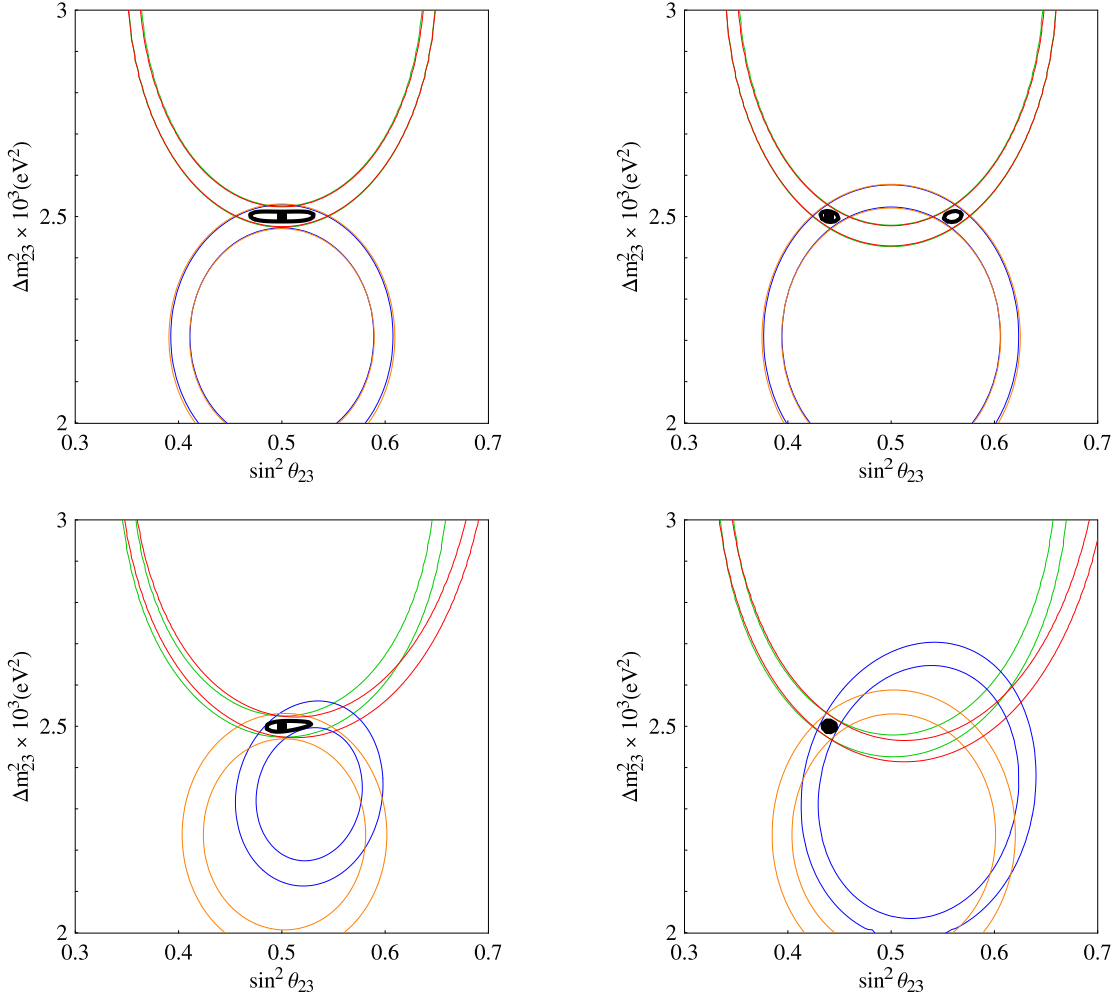


Fig. 13. *Binning at the $L = 7000$ km Neutrino Factory. Left: $\theta_{23} = 45^\circ$; right: $\theta_{23} = 41.5^\circ$; top: $\theta_{13} = 0^\circ$; bottom: $\theta_{13} = 8^\circ$.*

Factory combining both golden and silver appearance signal with the ν_μ disappearance signal, with no need for a huge water Čerenkov detector to be located somewhere else (albeit, using a 10 kton ECC).

The results of a four-parameters fit in $(\theta_{23}, \Delta m_{23}^2, \theta_{13}, \delta)$ projected onto the $(\theta_{23}, \Delta m_{23}^2)$ plane⁶ obtained by combining the disappearance and appearance signals at the Neutrino Factory are eventually presented in Fig. 14 for the medium baseline $L = 3000$ km and in Fig. 15 for the long baseline, $L = 7000$ km. Again, two values of $\bar{\theta}_{23}$, $\bar{\theta}_{23} = 41.5^\circ, 45^\circ$ (left and right panels, respectively) and two values of $\bar{\theta}_{13}$, $\bar{\theta}_{13} = 0^\circ, 8^\circ$ (top and bottom panels, respectively) are shown.

The input value for δ is $\bar{\delta} = 0^\circ$. In each figure, dotted lines refer to the fit with $\theta_{13} = \bar{\theta}_{13}$, $\delta = \bar{\delta}$ and $s_{atm} = \bar{s}_{atm}$. The solid lines, on the other hand, represent the result of a fit with variable θ_{13}, δ and s_{atm} . Notice that, as a general result, the uncertainties

⁶ The two-parameters 90 % CL contours are shown.

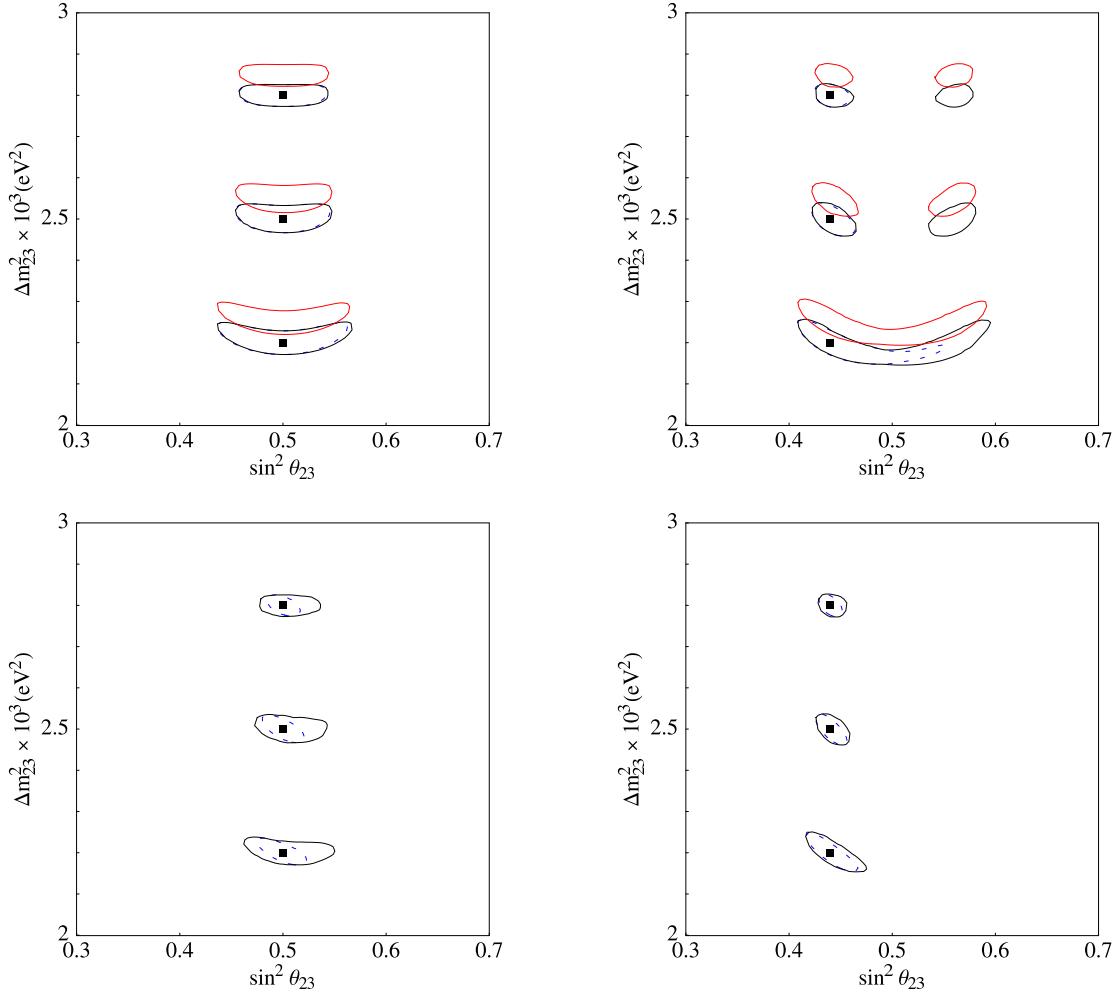


Fig. 14. *Appearance and disappearance in the $(\theta_{23}, \Delta m_{23}^2)$ plane at the $L = 3000$ km Neutrino Factory. Left: $\theta_{23} = 45^\circ$; right: $\theta_{23} = 41.5^\circ$; top: $\theta_{13} = 0^\circ$; bottom: $\theta_{13} = 8^\circ$.*

on the atmospheric parameters are better measured at the long baseline than at the medium one. In particular, for $\theta_{13} = 0^\circ$, maximal mixing cannot be excluded for a low atmospheric mass difference, $\Delta m_{23}^2 = 2.2 \times 10^{-3} \text{ eV}^2$ at the medium baseline: for such a low value of Δm_{23}^2 , all the energy bins are above-peak and thus show an upward-curved shape (see Fig. 12), reducing their complementarity. For $\theta_{13} = 8^\circ$ the octant ambiguity is always solved by the strong matter effects at both baselines. Combining the disappearance channel with the long-studied golden and silver appearance channels at the Neutrino Factory solves the octant-ambiguity for $\theta_{13} \geq 3^\circ$.

In Fig. 16 we eventually show the results of a four-parameters fit in $(\theta_{23}, \Delta m_{23}^2, \theta_{13}, \delta)$ projected onto the “classic” (θ_{13}, δ) plane [10] obtained by combining the disappearance and appearance signals at the Neutrino Factory, both for the $L = 3000$ km and $L = 7000$ km baselines (left and right panels, respectively). Two values of δ are shown, $\bar{\delta} = 45^\circ$ (top panels) and $\bar{\delta} = -90^\circ$ (bottom panels), and three values of θ_{13} , $\bar{\theta}_{13} = 2^\circ, 5^\circ$ and 8° (corresponding to $\sin \theta_{13} = 0.04, 0.09, 0.14$). Solid lines correspond to 90% CL

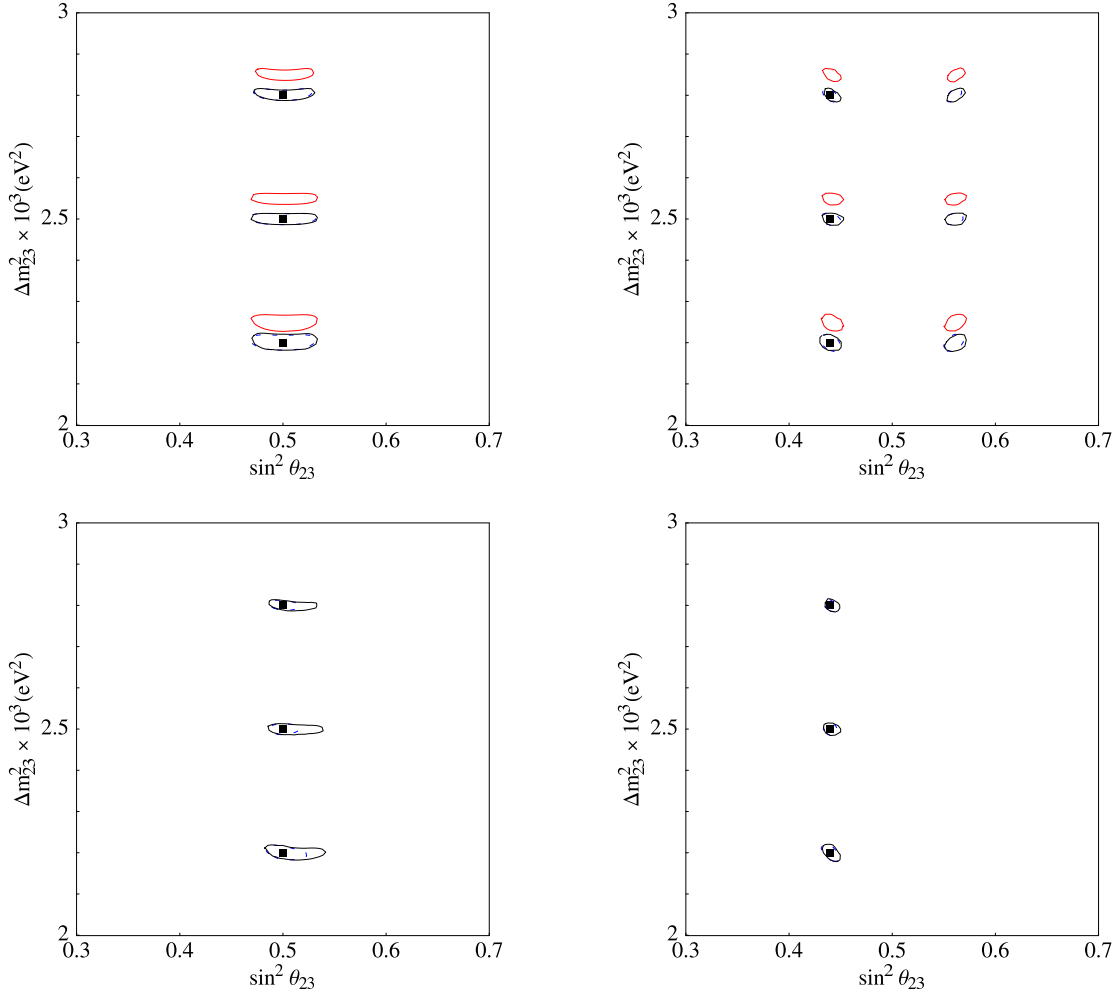


Fig. 15. *Appearance and disappearance in the $(\theta_{23}, \Delta m_{23}^2)$ plane at the $L = 7000$ km Neutrino Factory. Left: $\theta_{23} = 45^\circ$; right: $\theta_{23} = 41.5^\circ$; top: $\theta_{13} = 0^\circ$; bottom: $\theta_{13} = 8^\circ$.*

contours with $(s_{atm}, s_{oct}) = (\bar{s}_{atm}, \bar{s}_{oct})$, dashed lines to $(s_{atm}, s_{oct}) \neq (\bar{s}_{atm}, \bar{s}_{oct})$. As it has been known for long, the Neutrino Factory experiments have such a long baseline that the sign of the atmospheric mass difference is measured down to $\theta_{13} = 2^\circ$. The novelty here, is in that at 90 % CL not only the sign clones but the octant and intrinsic clones are also solved down to $\theta_{13} = 2^\circ$ for most values of δ . This stands true for both baselines. However, it is manifest that for $L = 7000$ km the sensitivity to δ is lost (this was called the “magic baseline” [30] precisely because around this distance the effect of δ in the $\nu_e \rightarrow \nu_\mu$ oscillation probability vanishes, see also Refs. [29] and [14]). A very good measurement of θ_{13} can be performed at this baseline, but certainly not of the leptonic CP-violating phase. The case of $\bar{\delta} = -90^\circ$ is particularly bad, due to low statistics in the antineutrino sample as opposed to a relatively high background. In this case the combination of neutrino and antineutrino fluxes is not as effective as for positive δ and the allowed region increases (something that has been observed for the β -Beam also, see Refs. [57,20]).

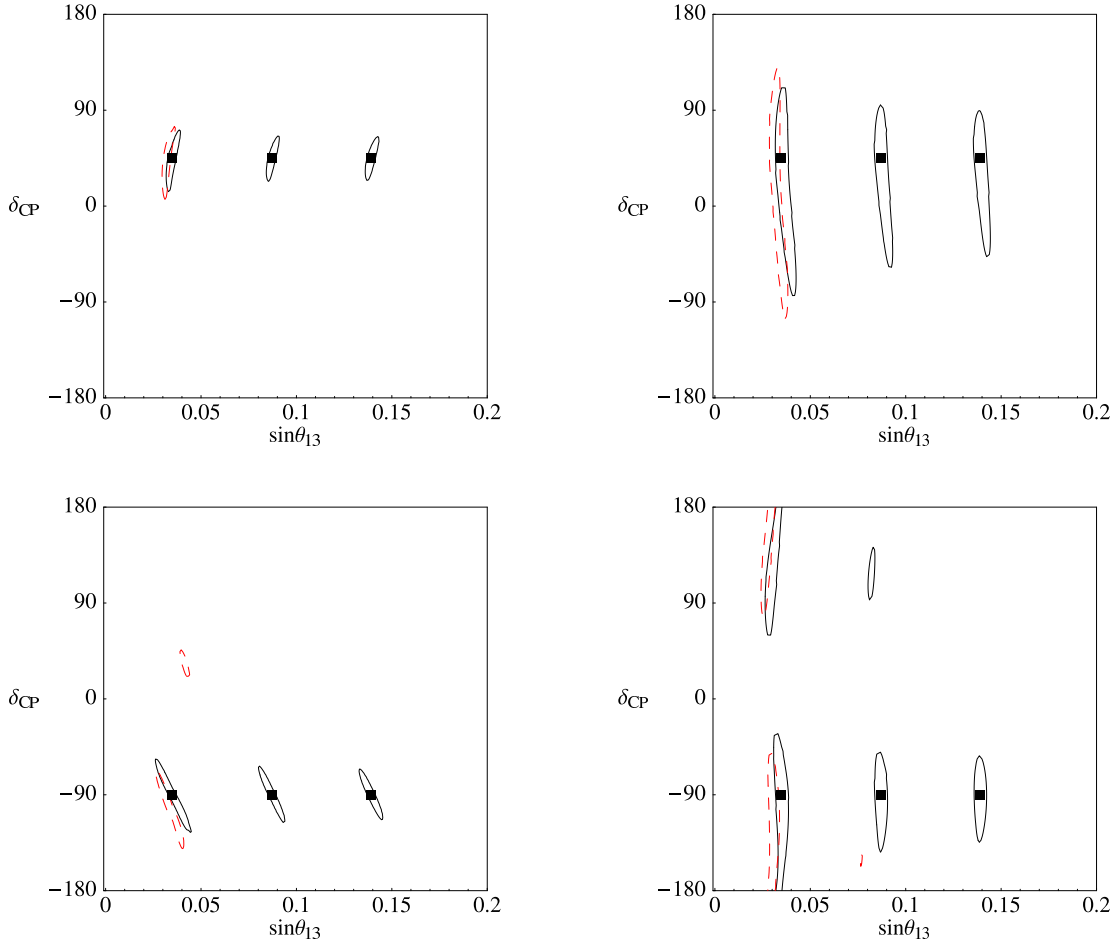


Fig. 16. *Appearance and disappearance in the (θ_{13}, δ) plane at the Neutrino Factory. Left: $L = 3000$ km baseline; right: $L = 7000$ km baseline; top: $\delta = 45^\circ$; bottom: $\delta = -90^\circ$. The mixing angle takes the following values: $\theta_{13} = 2^\circ, 5^\circ$ and 8° .*

5 Sensitivities

In this section we compare the sensitivities to θ_{13} , the maximality of θ_{23} , the sign of the atmospheric mass difference, the θ_{23} -octant, as well as the CP-discovery potential at the experimental facilities studied in this paper. Since T2K-I and NO ν A will run with neutrinos only, no sensitivity to the δ phase is expected; we then study them separately from the other facilities in section (Sect.5.1). The SPL, T2K-II and the Neutrino Factories with $L = 3000$ km and $L = 7000$ km will be analysed in Sect.5.2. All the contours have been computed adding the appearance and disappearance channels available at a given facility and, if not differently stated, all the parameters not involved in the fits are fixed to their best fit values as quoted in the Introduction.

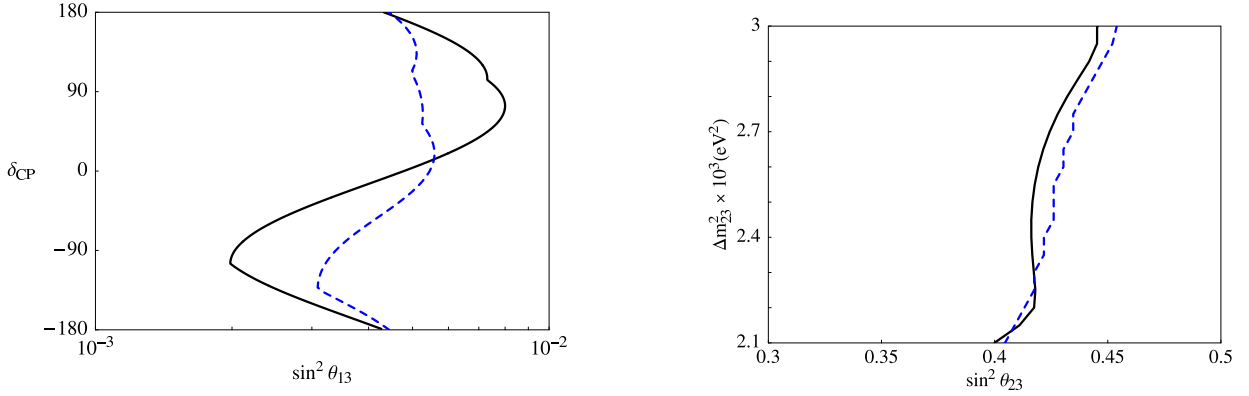


Fig. 17. *Left: 3σ θ_{13} -sensitivity; right: 3σ sensitivity to maximal θ_{23} . Solid lines refer to T2K-I; dashed lines to NO ν A.*

5.1 Sensitivities at T2K-I and NO ν A

In Fig.17 we compare the θ_{13} -sensitivity (left plot) and the sensitivity to maximal θ_{23} (right plots) at T2K-I (solid lines) and NO ν A (dashed lines).

- **θ_{13} -sensitivity**

The θ_{13} -sensitivity is defined as the one-parameter 3σ excluded region as a function of δ in case of absence of signal. The contours presented in the following figures represent the excluded values of θ_{13} for a given facility taking into account all possible choices of s_{atm} and s_{oct} . For both facilities the θ_{13} -sensitivity is rather poor, with a typical excluded region ranging from $[\sin^2 \theta_{13}]_{min} = [2, 8] \times 10^{-3}$. Sensitivity is slightly better for negative δ than for positive δ , with a maximal sensitivity at $\delta = -90^\circ (-135^\circ)$ for T2K (NO ν A). We have noticed that, while the T2K-I sensitivity is basically unaffected by the s_{atm} , s_{oct} choice, the NO ν A sensitivity is sensibly diminished in $\delta \in [-90^\circ, 90^\circ]$ when choosing a wrong value for the sign of Δm_{23}^2 or the θ_{23} -octant.

To increase both the θ_{13} -sensitivity and the CP-discovery potential it has been proposed to add a proton driver to the NO ν A design, such as to increase the neutrino flux from four to six times [24,38].

- **Sensitivity to maximal θ_{23}**

The potential to exclude maximal θ_{23} has been computed in the following way: for a given Δm_{23}^2 , we look for the largest value of θ_{23} for which the two-parameter 3σ contours do not touch $\theta_{23} = 45^\circ$. We have considered both octants of θ_{23} and we have found a behavior approximately symmetric of the sensitivity; we then display our results in the $\sin^2 \theta_{23}$ variable up to the maximal mixing value of 0.5.

As we can see in Fig.17 (right), the sensitivity for the two experiments is essentially the same and strongly decreases for low values of Δm_{23}^2 . At the best fit point $\Delta m_{23}^2 =$

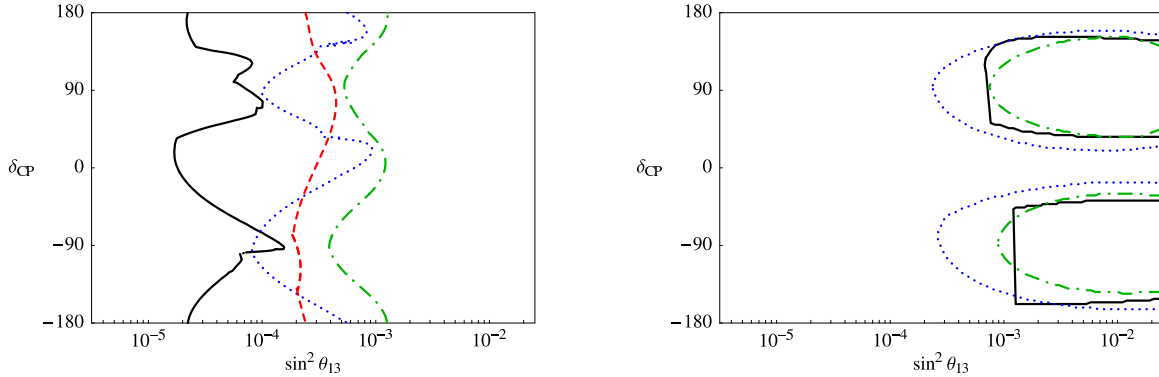


Fig. 18. *Left: 3σ θ_{13} -sensitivity; right: 3σ CP-discovery potential. Solid lines refer to the $L = 3000$ km Neutrino Factory; dashed lines to the $L = 7000$ km Neutrino Factory; dotted lines to T2K-II; dot-dashed lines to the (standard) SPL.*

2.5×10^{-3} eV² deviations as small as 14% of $\sin^2 \theta_{23}$ from maximal mixing could be established at both facilities. Notice that these curves have been computed for a fixed $\theta_{13} = 0$ (and $s_{atm} = +1$) so that matter effects in disappearance probabilities and those from the appearance channel $\nu_\mu \rightarrow \nu_e$ are completely negligible. We have also checked that for θ_{13} close to the current bound, none of the shown results changes drastically and that everything is basically independent on the mass hierarchy.

5.2 Sensitivities at T2K-II, SPL and Neutrino Factories

• θ_{13} -sensitivity and CP-discovery potential

In Fig.18 (left) we present the θ_{13} -sensitivity (computed as explained in the previous section) for T2K-II (dotted line), the SPL (dot-dashed line), the Neutrino Factory at $L = 3000$ (solid line) and $L = 7000$ (dashed line). As we can see, the NF at 3000 km shows the best sensitivity to θ_{13} in the whole range of δ (with the best value of $\sin^2 \theta_{13} \sim 2 \times 10^{-5}$ for δ around 30°) except a small region around $\delta = -90^\circ$ where T2K-II assures a slightly better performance (at the level of 8×10^{-5}). For the Neutrino Factory at $L = 7000$ km, the loss in sensitivity is to be ascribed to the sign degeneracy. For example, we have found that for $s_{atm} = \bar{s}_{atm}$ we get that θ_{13} is excluded at 3σ down to $\sin^2 \theta_{13} \sim 7 \times 10^{-5}$ ($\theta_{13} \sim 0.5^\circ$) if $\delta = 90^\circ$. On the other hand, for the same value of δ (but for a wrong choice of s_{atm}) we can only exclude θ_{13} down to $\sin^2 \theta_{13} \sim 4 \times 10^{-4}$ ($\theta_{13} \sim 1.1^\circ$). As for the SPL θ_{13} -sensitivity, the 3σ excluded region varies in the range $\sin^2 \theta_{13} \in [4 \times 10^{-4}, 1.5 \times 10^{-3}]$ for different values of δ , with no big differences coming from different choices of s_{atm} and s_{oct} . T2K-II is significantly better than the SPL but significantly worse than the NF at 3000 km, apart from $\delta = -90^\circ$ (where it improves a little the NF limit).

The CP-violation discovery potential has been computed as in Refs. [20,15]: at a fixed θ_{13} , we look for the smallest (largest) value of $|\bar{\delta}|$ for which the two-parameters 3σ contours of any of the degenerate solutions do not touch $\delta = 0^\circ$ nor $|\delta| = 180^\circ$. No-

tice that, although the input θ_{13} value is fixed, the degeneracies can touch $\delta = 0^\circ, 180^\circ$ at $\theta_{13} \neq \bar{\theta}_{13}$, also⁷. The outcome of this procedure is finally plotted, representing the region in the (θ_{13}, δ) parameter space for which a CP-violating signal is observed at 3σ . For each facility we show one single curve obtained taking into account the impact of all the degeneracies.

First of all, notice that no CP-discovery potential has been considered for the NF at 7000 km: due to matter effects and the choice of the baseline (close to the *magic baseline*, see Ref. [30]), the sensitivity to δ vanishes. The best sensitivity to the measurement of the CP-violating phase is reached by the T2K-II experiment: a CP-violating signal can be observed at 3σ for $|\delta| \in [27^\circ, 155^\circ]$ down to $\sin^2 \theta_{13} \sim 2 \times 10^{-4}$ ($\theta_{13} \sim 0.8^\circ$). At the SPL a good sensitivity can be reached also: CP violation is clearly observed at 3σ for $|\delta| \in [45^\circ, 135^\circ]$ down to $\sin^2 \theta_{13} \sim 9 \times 10^{-4}$ ($\theta_{13} \sim 1.7^\circ$), as it was shown in Ref. [20]. The NF at 3000 km is not as good as one would expect from its θ_{13} -sensitivity contours, having a CP-discovery potential very similar to the SPL; the loss in sensitivity with respect to T2K-II is mainly due to the presence of the sign degeneracy. We have observed that the NF starts to be insensitive to the leptonic CP-violation just when, for $\bar{\theta}_{13} \sim 2^\circ$, sign degeneracies close to $\theta_{13} = 0$ appear, which do not allow to exclude the CP-conserving case any longer. This is a consequence of the fact that, for neutrinos with $\langle E_\nu \rangle \sim 30$ GeV, the effective θ_{13} in matter [67,10] is extremely small. As it has been shown in Ref. [32], when θ_{13} vanishes, the sign degeneracies flow to $\delta = 0^\circ$ or $\delta = 180^\circ$, as can be seen in Figs. 2 and 3 (left) of Ref. [32]. At the SPL and T2K-II, for which the vacuum parameter θ_{13} is the relevant parameter, this happens at a much smaller value $\theta_{13} \sim 0.5^\circ$. Therefore, at these experiments the CP-discovery potential is statistics-dominated.

- **Sensitivity to the mass hierarchy**

In addition to the previous sensitivities one can ask for the sensitivity to the sign of the atmospheric mass difference. We compute the smallest values of θ_{13} for which the sign of Δm_{23}^2 can be measured in the $(\sin^2 \theta_{13}, \delta)$ plane. The measurement of s_{atm} requires matter effects to be sizeble. For this reason neither T2K-II nor the SPL have the capabilities to perform such a measurement. In Fig.19 we present the results for the Neutrino Factory only and for both possibilities of the true $s_{atm} = \pm 1$. As expected, the NF at 3000 km (solid and dotted lines for normal and inverted hierarchy, respectively) exhibits the worst sensitivity to $\text{sign}(\Delta m_{23}^2)$. For $s_{atm} = +1$ the best sensitivity is reached in a quite large region around $\delta = 90^\circ$ for which $[\sin^2 \theta_{13}]_{min} = 3.7 \times 10^{-4}$ (1.1°) whereas for $\delta \sim -90^\circ$ $[\sin^2 \theta_{13}]_{min} = 4 \times 10^{-3}$ (3.6°). The situation is completely reversed for $s_{atm} = -1$ due to the fact that in matter a

⁷ This is not the case of Fig. 11 in Ref. [57], where the excluded region in δ at fixed $\bar{\theta}_{13}$ in the absence of a CP-violating signal at 90% CL is presented. In practice, in that figure we compare $N_\pm(\bar{\theta}_{13}, \delta)$ with $N_\pm(\bar{\theta}_{13}, 0^\circ)$, thus obtaining a one-parameter sensitivity plot in δ only.

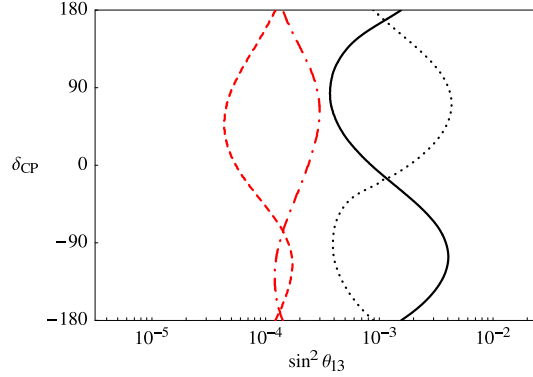


Fig. 19. 3σ sensitivity to the $\text{sign}(\Delta m_{23}^2)$. Solid lines refer to the $L = 3000$ km Neutrino Factory with normal hierarchy; dashed lines to the $L = 7000$ km Neutrino Factory with normal hierarchy; dotted lines to the $L = 3000$ km Neutrino Factory with inverted hierarchy; dot-dashed lines to the $L = 7000$ km Neutrino Factory with inverted hierarchy.

flip in the sign of Δm_{23}^2 corresponds to a change among neutrino and antineutrinos oscillation probabilities. At least one order of magnitude in sensitivity can be gained at the NF at 7000 km, depending on the fact that around $L=7000$ Km the effect of δ in the $\nu_e \rightarrow \nu_\mu$ oscillation probability vanishes and that helps to measure the sign of the atmospheric mass difference. For the normal hierarchy, a maximal sensitivity is achieved for $0 < \delta < 90^\circ$ at the level of $[\sin^2 \theta_{13}]_{\min} = 4.4 \times 10^{-5}$ (0.4°) whereas the largest value for $[\sin^2 \theta_{13}]_{\min} = 1.7 \times 10^{-4}$ (0.8°) is around $\delta = -100^\circ$. For the inverted hierarchy the sensitivity varies in the range $\sin^2 \theta_{13} \geq [1, 3] \times 10^{-4}$ ($0.6^\circ, 1^\circ$).

- **Sensitivity to maximal θ_{23} and the octant-discovery potential**

Eventually in Fig.20 we present the sensitivity to maximal θ_{23} (plot on the left) and the octant-discovery potential (plot on the right). The curves have been computed for $\theta_{13} = 0$.

With respect to the sensitivity to maximal θ_{23} , we observe that the NF at 3000 km (solid line) is not as good as one may expect since it measures far away from the oscillation maximum. At the value of Δm_{23}^2 in which the sensitivity is maximal, deviations as small as 10% of $\sin^2 \theta_{23}$ from maximal mixing could be established. Similar behaviour is expected at the SPL (dot-dashed line), except for small Δm_{23}^2 in which it outperforms the NF at 3000 km. A big improvement will be however achieved at a NF at 7000 km (dashed lines) and T2K-II (dotted line); both experiments have energies and baselines (as well as off-axis angle for T2K-II) chosen to match the first oscillation peak (in vacuum and matter respectively); the reached sensitivities are at the level of $\sin^2 \theta_{23} \in [0.45 - 0.48]$ almost independently on the value of Δm_{23}^2 , which means that deviations from maximal mixing of the order of 4% could be established.

Notice that, although this sensitivity is rather good, in general it is very difficult to determine the octant in which the atmospheric angle lies. As we can see from eq.(1), it is quite difficult to break the $\theta_{23} \rightarrow \pi/2 - \theta_{23}$ symmetry induced by the leading term in the transition probability; the subleading terms that could help in lifting this

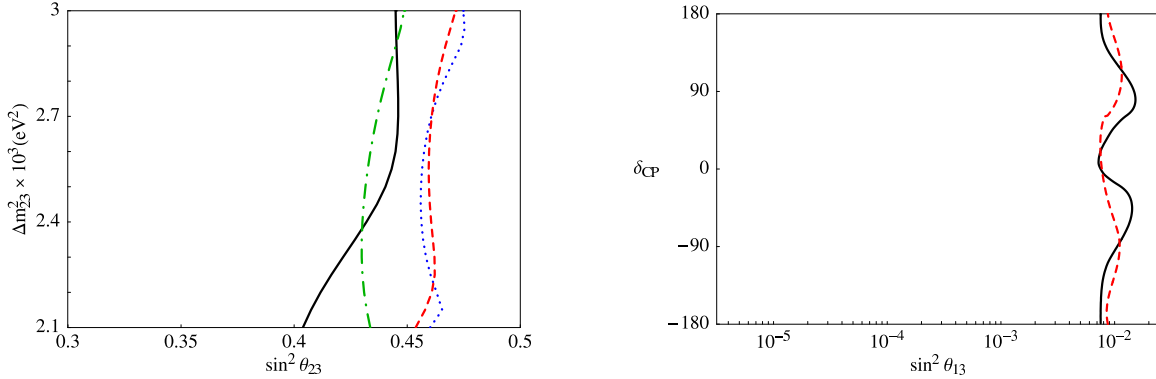


Fig. 20. *Left: 3σ sensitivity to maximal θ_{23} ; right: 3σ sensitivity to the θ_{23} -octant. Solid lines refer to the $L = 3000$ km Neutrino Factory; dashed lines to the $L = 7000$ km Neutrino Factory; dotted lines to T2K-II; dot-dashed lines to the (standard) SPL.*

degeneracy are very difficult to isolate. However, for values of θ_{13} different from zero, we can take full advantage of matter effects in the disappearance of muon neutrinos, as we have already seen in Sect.4 (Figs.12-13). Obviously the matter effects at SPL and T2K can never be sizeble enough to solve the octant ambiguity; on the other hand, the Neutrino Factory shows a (limited) capability to solve it, irrespective of the baseline and the value of δ . To illustrate this point, we fixed $\theta_{23} = 41.5^\circ$ and $\Delta m_{23}^2 = 2.5 \times 10^{-3} \text{ eV}^2$ and, for any value of δ , we compute the minimum value of θ_{13} for which the octant ambiguity is solved. As we can see in the right plot of Fig.20, a 3σ octant discovery is possible for $\sin^2 \theta_{23} > 0.01$ (6°).

6 Conclusions

In this paper, we studied the measurement of the atmospheric neutrino oscillation parameters, θ_{23} and Δm_{23}^2 using the ν_μ disappearance channel at three conventional beam facilities, the SPL, T2K-phase I and NO ν A, and at the Neutrino Factory. The precision on these two parameters will be of crucial importance in the measurement of two of the unknowns of the PMNS mixing matrix, θ_{13} and the leptonic CP-violating phase δ .

It has been shown that counting experiments cannot reduce significantly the uncertainties on θ_{23} and Δm_{23}^2 . Hence, we have considered detectors with (modest but non vanishing) sensitivity to the energy of the final leptons produced via neutrino interaction. For T2K-I and NO ν A we have indeed found that, independently of the input value of θ_{23} , the errors on θ_{23} can be significantly reduced. Different energy bins give different allowed regions in the $(\theta_{23}, \Delta m_{23}^2)$ -plane and the combination of them eventually helps in reducing the uncertainties around the physical point. The two experiments only run with π^+ , and thus are not sensitive to the CP-violating phase δ . The SPL, with a 1 Mton detector and 2 + 8 years of running time with π^+ and π^- , respectively, could in principle greatly improve these results. However, having neutrinos and antineutri-

nos at this setup does not help, since they have been produced with the same energy, roughly. Moreover, the baseline is too short for matter effects to make a difference. As a consequence, information coming from the two fluxes is not complementary and just add statistically. Remember, however, that this is not the case in the appearance mode, $\nu_\mu \rightarrow \nu_e$, for which this setup was designed. In this paper, we have considered two bins of energy at the SPL: this already makes a big difference in the precision on θ_{23} as it can be seen comparing with our results of Refs. [57,20] and [15], where only a counting experiment was considered for this facility.

We have then studied the impact of θ_{13} and δ in the measurement of θ_{23} and Δm_{23}^2 . Since both parameters are unknown at present, their values should be reconstructed at the same time with the atmospheric parameters. We have shown that the main effect of considering θ_{13} as a free variable is a shift of the contours toward larger values of θ_{23} (with respect to the input point) while a free δ in the whole $\delta \in [-180^\circ, 180^\circ]$ range does not produce any significant distortion of the allowed regions. These effects can be strongly softened if, in addition to the disappearance channels, we introduce in the analysis the appearance $\nu_\mu \rightarrow \nu_e$ channels, which the Super-Beam facilities have been proposed to look for. Two important conclusions can then be drawn: if θ_{13} is kept fixed, the combination of appearance and disappearance channels solves the *disappearance octant degeneracy* for θ_{13} large enough; on the other hand, the octant degeneracy is not lifted if θ_{13} is free to vary in the current allowed range, for almost any value of θ_{13} .

The situation is quite different at the Neutrino Factory. We have pointed out that the $\nu_\mu \rightarrow \nu_\mu$ disappearance channel is a very powerful tool to reduce the uncertainties on the atmospheric parameters up to an unprecedented level and, in combination with appearance channels, to solve many of the discrete ambiguities affecting the measurement of the PMNS matrix elements. The main feature emerging from such an analysis is that, for $\theta_{13} \geq 3^\circ - 4^\circ$, the synergy between disappearance and appearance channels (the more renowned *golden* and *silver* channels) greatly helps in solving the octant ambiguity, at both $L = 3000$ km and $L = 7000$ km baselines, as a result of the strong matter effects along the neutrino path and the huge statistics at hand. This remains true even in the case we leave θ_{13} as a free parameter, a situation which has been shown not to be true for the other facilities. Equally remarkable, in the same range of θ_{13} , the sign *clones* are solved and they are not present in the fits, independently of the baseline and the input values of θ_{23} and Δm_{23}^2 . This allows a precise measurement of θ_{13} at both facilities while the CP-phase δ , as it is already well known, can only be measured at $L = 3000$ Km. For values of $\theta_{13} \leq 3^\circ$, some remnant of the clones still remains and the measurement of the two unknowns cannot be performed with huge precision.

Eventually, we have presented a comparison at the different facilities of the 3σ sensitivity to θ_{13} , to maximal θ_{23} , to the mass hierarchy, to the θ_{23} -octant and their CP-discovery potential. T2K-I and NO ν A, running with neutrinos only are not able to measure δ . On the other hand, they have very similar performances in the θ_{13} -sensitivity, with an excluded region ranging from $[\sin^2 \theta_{13}]_{min} = 2 \times 10^{-3}$ to 8×10^{-3} ,

and in the sensitivity to maximal θ_{23} , with the maximal θ_{23} that can be distinguished from $\theta_{23} = 45^\circ$ ranging from $[\sin^2 \theta_{23}]_{max} = 0.45$ to 0.40 for $\Delta m_{23}^2 \in [2.0, 3.0] \times 10^{-3} \text{ eV}^2$.

The Neutrino Factory outperforms the considered Super-Beams for both baselines in the θ_{13} -sensitivity and in the sensitivity to the sign of the atmospheric mass difference. The longest baseline is as effective as T2K-II in the sensitivity to maximal θ_{23} . The excluded region in θ_{13} at the 3000 km Neutrino Factory ranges from $[\sin^2 \theta_{13}]_{min} = 2 \times 10^{-5}$ to 2×10^{-4} (for particular values of δ). The sign of the atmospheric mass difference can be measured at the 7000 Km (3000 Km) Neutrino Factory for $\sin^2 \theta_{13}$ as small as 10^{-4} (10^{-3}). Finally, the θ_{23} -octant can be identified at both facilities for $\sin^2 \theta_{13}$ as small as 10^{-2} ($\theta_{13} \geq 6^\circ$). Notably enough, the CP-discovery potential seems to be larger for T2K-II than for Neutrino Factory at $L = 3000 \text{ Km}$ (no CP-discovery potential is expected at the *magic baseline* $L = 7000 \text{ Km}$). This is explained as follows: as a general rule, for small values of θ_{13} the degeneracies flow toward $\delta = 0^\circ$ and $|\delta| = 180^\circ$ (see Ref. [32] and Ref. [31]), thus mimicking a non-CP violating phase. Due to a *parametric conspiracy* between the chosen energy and baseline and the matter effects, at the Neutrino Factory the typical value of θ_{13} for which this happens is much larger than at the SPL and T2K. Therefore, although from the statistical point of view the Neutrino Factory would certainly outperform both the SPL and T2K-II, in practice for small values of θ_{13} a CP-violating phase will be difficult to distinguish from a non-CP-violating one, if s_{atm} and s_{oct} are not measured previously.

Acknowledgments

We would like to thank E. Couce, B. Gavela, J. Gomez-Cadenas, P. Hernandez, P. Huber, O. Mena, P. Migliozzi, T. Schwetz and W. Winter for useful discussions. The authors acknowledge the financial support of MCYT through project FPA2003-04597 and of the European Union through the networking activity BENE. E.F. acknowledges financial support from the UAM.

Appendix A

In this Appendix we recall the number of events per bin that are expected in the $\nu_\mu(\bar{\nu}_\mu)$ disappearance channel at the SPL, the T2K-I, the NO ν A and the Neutrino Factory experiments. The expected T2K-I muon and electron identification efficiencies are presented, as well.

In all tables, two different values of θ_{13} and δ are considered, as well as two choices of $\text{sign}(\Delta m_{23}^2)$.

In Tab. 1 we show the expected event rates per bin at the SPL after a 2 years run with π^+ and a 8 years run with π^- , using the fluxes of Ref. [41] and a 440 kt detector at

$L = 130$ km.

$E_\nu \in [0, 250]$ MeV	No Osc.	$\theta_{13} = 0^\circ$	$\theta_{13} = 8^\circ; \delta = 0^\circ$	$\theta_{13} = 8^\circ; \delta = 90^\circ$
$N_{\mu^-, s_{atm}} = +$	2784	186	198	192
$N_{\mu^-, s_{atm}} = -$		158	158	162
$E_\nu \in [250, 600]$ MeV	No Osc.	$\theta_{13} = 0^\circ$	$\theta_{13} = 8^\circ; \delta = 0^\circ$	$\theta_{13} = 8^\circ; \delta = 90^\circ$
$N_{\mu^-, s_{atm}} = +$	21461	2401	2423	2455
$N_{\mu^-, s_{atm}} = -$		2591	2682	2642
$E_{\bar{\nu}} \in [0, 250]$ MeV	No Osc.	$\theta_{13} = 0^\circ$	$\theta_{13} = 8^\circ; \delta = 0^\circ$	$\theta_{13} = 8^\circ; \delta = 90^\circ$
$N_{\mu^+, s_{atm}} = +$	6310	830	859	841
$N_{\mu^+, s_{atm}} = -$		740	737	753
$E_{\bar{\nu}} \in [250, 600]$ MeV	No Osc.	$\theta_{13} = 0^\circ$	$\theta_{13} = 8^\circ; \delta = 0^\circ$	$\theta_{13} = 8^\circ; \delta = 90^\circ$
$N_{\mu^+, s_{atm}} = +$	19157	1708	1734	1757
$N_{\mu^+, s_{atm}} = -$		1858	1939	1906

Table 1

Disappearance event rates for a 2 + 8 years $\pi^+ + \pi^-$ run at the standard SPL, for different values of θ_{13}, δ and of the sign of the atmospheric mass difference, s_{atm} .

In Tab. 2 we show the expected event rates for the two lowest bins at T2K-I after a 5 years run with π^+ , for a 22.5 kt detector at $L = 295$ km.

$E_\nu \in [400, 600]$ MeV	No Osc.	$\theta_{13} = 0^\circ$	$\theta_{13} = 8^\circ; \delta = 0^\circ$	$\theta_{13} = 8^\circ; \delta = 90^\circ$
$N_{\mu^-, s_{atm}} = +$	752	52	56	54
$N_{\mu^-, s_{atm}} = -$		45	46	47
$E_\nu \in [600, 800]$ MeV	No Osc.	$\theta_{13} = 0^\circ$	$\theta_{13} = 8^\circ; \delta = 0^\circ$	$\theta_{13} = 8^\circ; \delta = 90^\circ$
$N_{\mu^-, s_{atm}} = +$	2218	122	126	128
$N_{\mu^-, s_{atm}} = -$		140	149	145

Table 2

Disappearance event rates for a 5 years π^+ run at T2K-I, for different values of θ_{13}, δ and of the sign of the atmospheric mass difference, s_{atm} .

In Tab. 3 we show the expected event rates per bin at NO ν A after a 5 years run with π^+ , for a 30 kt detector at $L = 812$ km.

In Tabs. 4 and 5 we show the expected event rates per bin after a 5 years run with μ^- and a 5 years run with μ^+ at the Neutrino Factory, for a 40 kt detector at $L = 3000$ and $L = 7000$ km, respectively.

$E_\nu \in [1000, 1666]$ MeV	No Osc.	$\theta_{13} = 0^\circ$	$\theta_{13} = 8^\circ; \delta = 0^\circ$	$\theta_{13} = 8^\circ; \delta = 90^\circ$
$N_{\mu^-, s_{atm}} = +$	1217	120	125	116
$N_{\mu^-, s_{atm}} = -$		105	102	107
$E_\nu \in [1666, 2333]$ MeV	No Osc.	$\theta_{13} = 0^\circ$	$\theta_{13} = 8^\circ; \delta = 0^\circ$	$\theta_{13} = 8^\circ; \delta = 90^\circ$
$N_{\mu^-, s_{atm}} = +$	8635	819	800	847
$N_{\mu^-, s_{atm}} = -$		920	949	907
$E_\nu \in [2333, 3000]$ MeV	No Osc.	$\theta_{13} = 0^\circ$	$\theta_{13} = 8^\circ; \delta = 0^\circ$	$\theta_{13} = 8^\circ; \delta = 90^\circ$
$N_{\mu^-, s_{atm}} = +$	7545	1909	1886	1938
$N_{\mu^-, s_{atm}} = -$		2021	2048	2003

Table 3

Disappearance event rates for a 5 years π^+ run at NO ν A, for different values of θ_{13}, δ and of the sign of the atmospheric mass difference, s_{atm} .

$E_\nu \in [4, 8]$ GeV	No Osc.	$\theta_{13} = 0^\circ$	$\theta_{13} = 8^\circ; \delta = 0^\circ$	$\theta_{13} = 8^\circ; \delta = 90^\circ$
$N_{\mu^-, s_{atm}} = +$	6546	407	449	441
$N_{\mu^-, s_{atm}} = -$		418	430	426
$E_\nu \in [8, 12]$ GeV	No Osc.	$\theta_{13} = 0^\circ$	$\theta_{13} = 8^\circ; \delta = 0^\circ$	$\theta_{13} = 8^\circ; \delta = 90^\circ$
$N_{\mu^+, s_{atm}} = +$	26110	6608	6727	6776
$N_{\mu^+, s_{atm}} = -$		6914	7034	7004
$E_\nu \in [4, 8]$ GeV	No Osc.	$\theta_{13} = 0^\circ$	$\theta_{13} = 8^\circ; \delta = 0^\circ$	$\theta_{13} = 8^\circ; \delta = 90^\circ$
$N_{\mu^-, s_{atm}} = +$	3014	187	186	188
$N_{\mu^-, s_{atm}} = -$		192	210	210
$E_\nu \in [8, 12]$ GeV	No Osc.	$\theta_{13} = 0^\circ$	$\theta_{13} = 8^\circ; \delta = 0^\circ$	$\theta_{13} = 8^\circ; \delta = 90^\circ$
$N_{\mu^+, s_{atm}} = +$	12201	3092	3123	3136
$N_{\mu^+, s_{atm}} = -$		3232	3328	3305

Table 4

Disappearance event rates for a 5 + 5 years run at the $L = 3000$ km Neutrino Factory, for different values of θ_{13}, δ and of the sign of the atmospheric mass difference, s_{atm} .

Eventually, in Fig. 21 we present the muon (solid) and electron (dashed) identification efficiencies at the T2K-I experiment, as found in Ref. [68] and [16], respectively.

$E_\nu \in [10, 15]$ GeV	No Osc.	$\theta_{13} = 0^\circ$	$\theta_{13} = 8^\circ; \delta = 0^\circ$	$\theta_{13} = 8^\circ; \delta = 90^\circ$
$N_{\mu^-, s_{atm} = +}$	11129	639	438	413
$N_{\mu^-, s_{atm} = -}$		551	515	519
$E_\nu \in [15, 20]$ GeV	No Osc.	$\theta_{13} = 0^\circ$	$\theta_{13} = 8^\circ; \delta = 0^\circ$	$\theta_{13} = 8^\circ; \delta = 90^\circ$
$N_{\mu^+, s_{atm} = +}$	27181	2114	2582	2556
$N_{\mu^+, s_{atm} = -}$		2374	2565	2578
$E_\nu \in [10, 15]$ GeV	No Osc.	$\theta_{13} = 0^\circ$	$\theta_{13} = 8^\circ; \delta = 0^\circ$	$\theta_{13} = 8^\circ; \delta = 90^\circ$
$N_{\mu^-, s_{atm} = +}$	5225	299	269	268
$N_{\mu^-, s_{atm} = -}$		259	206	216
$E_\nu \in [15, 20]$ GeV	No Osc.	$\theta_{13} = 0^\circ$	$\theta_{13} = 8^\circ; \delta = 0^\circ$	$\theta_{13} = 8^\circ; \delta = 90^\circ$
$N_{\mu^+, s_{atm} = +}$	12799	997	1083	1077
$N_{\mu^+, s_{atm} = -}$		1116	1334	1345

Table 5

Disappearance event rates for a 5 + 5 years run at the $L = 7000$ km Neutrino Factory, for different values of θ_{13}, δ and of the sign of the atmospheric mass difference, s_{atm} .

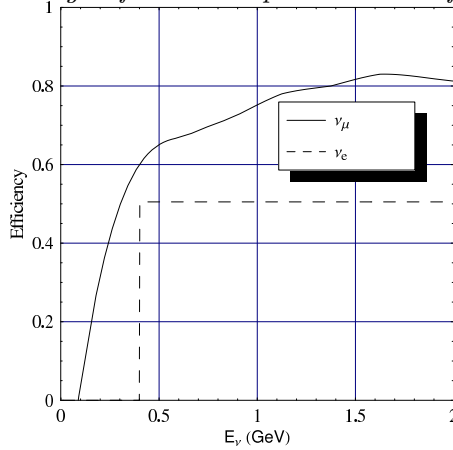


Fig. 21. Muon (solid) and electron (dashed) identification efficiency at T2K-I as a function of the neutrino energy.

References

- [1] Y. Fukuda *et al.* [Super-Kamiokande Collaboration], Phys. Rev. Lett. **81** (1998) 1562 [arXiv:hep-ex/9807003]; M. Ambrosio *et al.* [MACRO Collaboration], Phys. Lett. B **517** (2001) 59 [arXiv:hep-ex/0106049]; M. H. Ahn *et al.* [K2K Collaboration], Phys. Rev. Lett. **90** (2003) 041801 [arXiv:hep-ex/0212007]; B. T. Cleveland *et al.*, Astrophys. J. **496** (1998) 505; J. N. Abdurashitov *et al.* [SAGE Collaboration], Phys. Rev. C **60** (1999)

- 055801 [arXiv:astro-ph/9907113]; W. Hampel *et al.* [GALLEX Collaboration], Phys. Lett. B **447** (1999) 127; S. Fukuda *et al.* [Super-Kamiokande Collaboration], Phys. Rev. Lett. **86** (2001) 5651 [arXiv:hep-ex/0103032]; Q. R. Ahmad *et al.* [SNO Collaboration], Phys. Rev. Lett. **87** (2001) 071301 [arXiv:nucl-ex/0106015]; K. Eguchi *et al.* [KamLAND Collaboration], Phys. Rev. Lett. **90** (2003) 021802 [arXiv:hep-ex/0212021].
- [2] C. Athanassopoulos *et al.* [LSND Collaboration], Phys. Rev. Lett. **81** (1998) 1774 [arXiv:nucl-ex/9709006]; A. Aguilar *et al.* [LSND Collaboration], Phys. Rev. D **64** (2001) 112007 [arXiv:hep-ex/0104049].
- [3] I. Stancu *et al.* [MiniBooNE collaboration], FERMILAB-TM-2207.
- [4] B. Pontecorvo, Sov. Phys. JETP **6** (1957) 429 [Zh. Eksp. Teor. Fiz. **33** (1957) 549]; Z. Maki, M. Nakagawa and S. Sakata, Prog. Theor. Phys. **28** (1962) 870; B. Pontecorvo, Sov. Phys. JETP **26** (1968) 984 [Zh. Eksp. Teor. Fiz. **53** (1967) 1717]; V. N. Gribov and B. Pontecorvo, Phys. Lett. B **28** (1969) 493.
- [5] M. Apollonio *et al.* [CHOOZ Collaboration], Phys. Lett. B **466** (1999) 415 [arXiv:hep-ex/9907037]; Eur. Phys. J. C **27** (2003) 331 [arXiv:hep-ex/0301017].
- [6] G. L. Fogli, E. Lisi, A. Marrone and A. Palazzo, arXiv:hep-ph/0506083; G. L. Fogli, E. Lisi, A. Marrone, A. Palazzo and A. M. Rotunno, arXiv:hep-ph/0506307.
- [7] H. Pessard [OPERA Collaboration], arXiv:hep-ex/0504033; M. Guler *et al.* [OPERA Collaboration], “OPERA: An appearance experiment to search for $\nu_\mu \rightarrow \nu_\tau$ oscillations in the CNGS beam. Experimental proposal,” CERN-SPSC-2000-028.
- [8] F. Arneodo *et al.*, Nucl. Instrum. Meth. A **461** (2001) 324. P. Aprili *et al.* [ICARUS Collaboration], CERN-SPSC-2002-027.
- [9] S. N. Ahmed *et al.* [SNO Collaboration], Phys. Rev. Lett. **92** (2004) 181301 [arXiv:nucl-ex/0309004].
- [10] A. Cervera, A. Donini, M. B. Gavela, J. J. Gomez Cadenas, P. Hernandez, O. Mena and S. Rigolin, Nucl. Phys. B **579** (2000) 17 [Erratum-ibid. B **593** (2001) 731] [arXiv:hep-ph/0002108].
- [11] J. Burguet-Castell, M. B. Gavela, J. J. Gomez-Cadenas, P. Hernandez and O. Mena, Nucl. Phys. B **608** (2001) 301 [arXiv:hep-ph/0103258].
- [12] H. Minakata and H. Nunokawa, JHEP **0110** (2001) 001 [arXiv:hep-ph/0108085].
- [13] G. L. Fogli and E. Lisi, Phys. Rev. D **54** (1996) 3667 [arXiv:hep-ph/9604415].
- [14] V. Barger, D. Marfatia and K. Whisnant, Phys. Rev. D **65** (2002) 073023 [arXiv:hep-ph/0112119].
- [15] A. Donini, D. Meloni and S. Rigolin, arXiv:hep-ph/0506100; D. Meloni, Acta Phys. Polon. B **35** (2004) 2781; arXiv:hep-ph/0509370.
- [16] Y. Itow *et al.*, arXiv:hep-ex/0106019.

- [17] P. Zucchelli, Phys. Lett. B **532** (2002) 166.
- [18] S. Geer, Phys. Rev. D **57** (1998) 6989 [Erratum-ibid. D **59** (1999) 039903] [arXiv:hep-ph/9712290]; A. De Rujula, M. B. Gavela and P. Hernandez, Nucl. Phys. B **547** (1999) 21 [arXiv:hep-ph/9811390].
- [19] C. Albright *et al.*, arXiv:hep-ex/0008064; M. Apollonio *et al.*, arXiv:hep-ph/0210192.
- [20] A. Donini, E. Fernández-Martínez and S. Rigolin, Phys. Lett. B **621**, 276 (2005) [arXiv:hep-ph/0411402]; S. Rigolin, arXiv:hep-ph/0411403.
- [21] P. Huber, M. Maltoni and T. Schwetz, Phys. Rev. D **71** (2005) 053006 [arXiv:hep-ph/0501037].
- [22] S. Choubey and P. Roy, arXiv:hep-ph/0509197.
- [23] A. Donini, E. Fernández-Martínez and S. Rigolin, arXiv:hep-ph/0509349.
- [24] D. S. Ayres *et al.* [NOvA Collaboration], arXiv:hep-ex/0503053.
- [25] J. J. Gomez-Cadenas *et al.* [CERN working group on Super Beams Collaboration], arXiv:hep-ph/0105297.
- [26] V. D. Barger, S. Geer, R. Raja and K. Whisnant, Phys. Rev. D **62** (2000) 013004 [arXiv:hep-ph/9911524].
- [27] A. Bueno, M. Campanelli and A. Rubbia, Nucl. Phys. B **589** (2000) 577 [arXiv:hep-ph/0005007].
- [28] A. Donini, D. Meloni and P. Migliozzi, Nucl. Phys. B **646** (2002) 321 [arXiv:hep-ph/0206034]; J. Phys. G **29** (2003) 1865 [arXiv:hep-ph/0209240].
- [29] A. Donini, M. B. Gavela, P. Hernandez and S. Rigolin, Nucl. Phys. B **574** (2000) 23 [arXiv:hep-ph/9909254].
- [30] P. Huber and W. Winter, Phys. Rev. D **68** (2003) 037301 [arXiv:hep-ph/0301257].
- [31] J. Burguet-Castell, M. B. Gavela, J. J. Gomez-Cadenas, P. Hernandez and O. Mena, Nucl. Phys. B **646** (2002) 301 [arXiv:hep-ph/0207080].
- [32] A. Donini, D. Meloni and S. Rigolin, JHEP **0406**, 011 (2004) [arXiv:hep-ph/0312072].
- [33] T. Nakaya, Nucl. Phys. Proc. Suppl. **143** (2005) 96.
- [34] S. E. Kopp, AIP Conf. Proc. **773**, 276 (2005) [arXiv:hep-ex/0412052].
- [35] K. Kodama [OPERA Collaboration], AIP Conf. Proc. **721** (2004) 231.
- [36] P. Huber, M. Lindner and W. Winter, Comput. Phys. Commun. **167** (2005) 195 [arXiv:hep-ph/0407333].
- [37] M. G. Albrow *et al.*, arXiv:hep-ex/0509019.

- [38] O. Mena Requejo, S. Palomares-Ruiz and S. Pascoli, Phys. Rev. D **72**, 053002 (2005) [arXiv:hep-ph/0504015]; O. Mena and S. Parke, Phys. Rev. D **72** (2005) 053003 [arXiv:hep-ph/0505202]; O. Mena, S. Palomares-Ruiz and S. Pascoli, arXiv:hep-ph/0510182.
- [39] P. Huber, M. Lindner and W. Winter, Nucl. Phys. B **654** (2003) 3 [arXiv:hep-ph/0211300].
- [40] H. Budd, arXiv:hep-ex/0503024.
- [41] S. Gilardoni, CERN Thesis; S. Gilardoni, G. Grawer, G. Maire, J. M. Maugain, S. Rangod and F. Voelker, J. Phys. G **29** (2003) 1801.
- [42] J. E. Campagne and A. Cazes, arXiv:hep-ex/0411062.
- [43] C. K. Jung, arXiv:hep-ex/0005046.
- [44] J. Burguet-Castell, D. Casper, J. J. Gomez-Cadenas, P. Hernandez and F. Sanchez, Nucl. Phys. B **695**, 217 (2004) [arXiv:hep-ph/0312068].
- [45] A. Blondel, M. Campanelli and M. Fechner, Nucl. Instrum. Meth. A **535** (2004) 665.
- [46] D. Casper, Nucl. Phys. Proc. Suppl. **112** (2002) 161 [arXiv:hep-ph/0208030].
- [47] A. Blondel *et al.*, Nucl. Instrum. Meth. A **451** (2000) 102.
- [48] A. Cervera, F. Dydak and J. Gomez Cadenas, Nucl. Instrum. Meth. A **451** (2000) 123.
- [49] D. Autiero *et al.*, Eur. Phys. J. C **33** (2004) 243 [arXiv:hep-ph/0305185].
- [50] G. P. Zeller, arXiv:hep-ex/0312061.
- [51] P. Lipari, private communication; P. Lipari, M. Lusignoli and F. Sartogo, Phys. Rev. Lett. **74**, 4384 (1995) [arXiv:hep-ph/9411341].
- [52] J. Serreau and C. Volpe, Phys. Rev. C **70**, 055502 (2004) [arXiv:hep-ph/0403293].
- [53] D. A. Petyt, FERMILAB-THESIS-1998-66
- [54] H. Minakata, M. Sonoyama and H. Sugiyama, Phys. Rev. D **70**, 113012 (2004) [arXiv:hep-ph/0406073].
- [55] E. K. Akhmedov *et al.*, JHEP **0404** (2004) 078 [arXiv:hep-ph/0402175].
- [56] G. L. Fogli, E. Lisi and A. Palazzo, Phys. Rev. D **65** (2002) 073019 [arXiv:hep-ph/0105080].
- [57] A. Donini, E. Fernández-Martínez, P. Migliozzi, S. Rigolin and L. Scotto Lavina, Nucl. Phys. B **710** (2005) 402 [arXiv:hep-ph/0406132]; S. Rigolin, arXiv:hep-ph/0407009.
- [58] H. Minakata, H. Nunokawa and S. J. Parke, Phys. Rev. D **68** (2003) 013010 [arXiv:hep-ph/0301210]; M. Ishitsuka, T. Kajita, H. Minakata and H. Nunokawa, Phys. Rev. D **72** (2005) 033003 [arXiv:hep-ph/0504026]; arXiv:hep-ph/0510166.

- [59] O. Yasuda, *New J. Phys.* **6** (2004) 83 [arXiv:hep-ph/0405005]; *Nucl. Phys. Proc. Suppl.* **149** (2005) 170 [arXiv:hep-ph/0412405].
- [60] J. Bouchez, M. Lindroos and M. Mezzetto, *AIP Conf. Proc.* **721** (2004) 37 [arXiv:hep-ex/0310059]; M. Mezzetto, *Nucl. Phys. Proc. Suppl.* **143** (2005) 309 [arXiv:hep-ex/0410083].
- [61] F. Terranova, A. Marotta, P. Migliozi and M. Spinetti, *Eur. Phys. J. C* **38**, 69 (2004) [arXiv:hep-ph/0405081].
- [62] J. Burguet-Castell, D. Casper, E. Couce, J. J. Gomez-Cadenas and P. Hernandez, *Nucl. Phys. B* **725**, 306 (2005) [arXiv:hep-ph/0503021].
- [63] P. Huber, M. Lindner, M. Rolinec and W. Winter, arXiv:hep-ph/0506237.
- [64] S. Rigolin, arXiv:hep-ph/0509366.
- [65] A. Donini, E. Fernández-Martínez, P. Migliozi, S. Rigolin, L. Scotto Lavina, T. T. de Fatis and F. Terranova, arXiv:hep-ph/0511134.
- [66] A. Donini, *AIP Conf. Proc.* **721**, 219 (2004) [arXiv:hep-ph/0310014].
- [67] H. W. Zaglauer and K. H. Schwarzer, *Z. Phys. C* **40** (1988) 273.
- [68] P. Migliozi, private communication.